Hochhaus A, Saglio G, Larson RA, Kim DW, Etienne G, Rosti G, De Souza C, Kurokawa M, Kalaycio ME, Hoenekopp A, Fan X, Shou Y, Kantarjian HM, Hughes TP	Nilotinib is associated with a reduced incidence of BCR-ABL mutations vs imatinib in patients with newly diagnosed chronic myeloid leukemia in chronic phase.	Blood	121	3703-8	2013
Shimizu K, Yamagata K, Kurokawa M, Mizutani S, Tsunematsu Y, Kitabayashi I	Roles of AML1/RUNX1 in T-cell malignancy induced by loss of p53.	Cancer Sci	104	1033-8	2013
脇　裕典	糖尿病と遺伝子 4. 糖尿病とエピゲノム.	糖尿病	57(2)	91-93	2014
山内敏正, 岩部美紀, 岩部真人, 門脇孝	アカデミア創薬研究の今を知る《各疾患領域におけるニーズと研究戦略》 11.代謝疾患の治療に向けたアカデミア創薬—アディポネクチン受容体を標的とした健康長寿薬開発への挑戦.	実験医学	32(2)	343-350	2014
山内敏正, 門脇孝	脂肪由来のホルモン　アディポネクチン.	月刊内分泌・糖尿病・代謝内科	36	451-457	2013
脇裕典, 山内敏正, 植木浩二郎, 門脇孝	明らかになる褐色脂肪組織の機能:今,第三の細胞が目覚める ヒト褐色脂肪細胞の細胞系譜 古典的褐色脂肪細胞か,ベージュ/Brite 細胞か?	細胞工学	32(7)	759-762	2013
脇裕典, 山内敏正, 門脇孝	核内受容体 PPAR と脂肪酸.	月刊内分泌・糖尿病・	36(6)	558-56	2013
Morita H	Human genomics in cardiovascular medicine:implications and	Circ J	77(4)	876-885	2013
森田啓行	iPS 細胞を用いた心不全の病態解析	Pharma Medica	31(5)	45-48	2013
Morita H, Komuro I	A novel channelopathy in pulmonary arterial hypertension.	N Engl J Med	369(22)	2161-2162	2013

Morita H	Genetic variants and dilated cardiomyopathy – To be or not to be causative: Is that the question? –	Circ J	77(12)	2879-2880	2013
森田啓行	遺伝子から心筋症をみる.	日内会誌	103(2)	285-292	2014
Nasuno M, Arimura Y, Nagaishi K, Isshiki H, Onodera K, Nakagaki S, Watanabe S, Idogawa M, Yamashita K, Naishiro Y, Adachi Y, Suzuki H, Fujimiya M, Imai K, Shinomura Y.	Mesenchymal stem cells cancel azoxymethane-induced tumor initiation.	STEM CELLS n/a–n/a DOI	10.1002/stem	1594	2013
Suzuki R, Yamamoto E, Nojima M, Maruyama R, Yamano HO, Yoshikawa K, Kimura T, Harada T, Ashida M, Niinuma T, Sato A, Nosho K, Yamamoto H, Kai M, Sugai T, Imai K, Suzuki H, Shinomura Y.	Aberrant methylation of microRNA-34b/c is a predictive marker of metachronous gastric cancer risk.	J Gastroenterol	[Epub ahead of print]		2013
Shimizu T, Suzuki H, Nojima M, Kitamura H, Yamamoto E, Maruyama R, Ashida M, Hatahira T, Kai M, Masumori N, Tokino T, Imai K, Tsukamoto T, Toyota M.	Methylation of a panel of microRNA genes is a novel biomarker for detection of bladder cancer.	Eur Urol	63	1091-1100	2013
Sawada T, Yamamoto E, Suzuki H, Nojima M, Maruyama R, Shioi Y, Akasaka R, Kamimae S, Harada T, Ashida M, Kai M, Adachi Y, Yamamoto H, Imai K, Toyota M, Itoh F, Sugai T.	Association between genomic alterations and metastatic behavior of colorectal cancer identified by array-based comparative genomic hybridization.	Genes Chromosomes Cancer	52	140-149	2013
Kato N, Yamamoto H, Adachi Y, Ohashi H, Taniguchi H, Suzuki H, Nakazawa M, Kaneto H, Sasaki S, Imai K, Shinomura Y.	Cancer detection by ubiquitin carboxyl-terminal esterase L1 methylation in pancreatobiliary fluids.	World J Gastroenterol	19	1718-1727	2013

Adachi Y, Ohashi H, Imsumran A, Yamamoto H, Matsunaga Y, Taniguchi H, Nosho K, Suzuki H, Sasaki Y, Arimura Y, Carbone DP, Imai K, Shinomura Y.	The effect of IGF-I receptor blockade for human esophageal squamous cell carcinoma and adenocarcinoma.	Tumor Biol	[Epub ahead of print		2013
Watanabe S, Arimura Y, Nagaishi K, Isshiki H, Onodera K, Nasuno M, Yamashita K, Idogawa M, Naishiro Y, Murata M, Adachi Y, Fujimiya M, Imai K, Shinomura Y.	Conditioned mesenchymal stem cells produce pleiotropic gut trophic factors.	J Gastroenterol	Nov 12. [Epub ahead of print]		2013
Arimura Y, Isshiki H, Onodera K, Nagaishi K, Yamashita K, Sonoda T, Matsumoto T, Takahashi A, Takazoe M, Yamazaki K, Kubo M, Fujimiya M, Imai K, Shinomura Y.	Characteristics of Japanese inflammatory bowel disease susceptibility loci.	J Gastroenterol	Aug 13. [Epub ahead of print]		2013
Adachi E, Kogayu M, Fjii T, Mae H, Shimizu H, Iwai Y, Shibata H, Suzuki M, Imai K, Koibuchi T.	Tuberculosis examination using whole blood interferon-gamma release assay among health care workers in a Japanese hospital without tuberculosis-specific wards.	SpringerPlus	2:440(05 Sep)		2013
Ito M, Mitsuhashi K, Igarashi H, Nosho K, Naito T, Yoshii S, Takahashi H, Fujita M, Sukawa Y, Yamamoto E, Takahashi T, Adachi Y, Nojima M, Sasaki Y, Tokino T, Baba T, Maruyama R, Suzuki H, Imai K, Yamamoto H, Shinomura Y.	MicroRNA-31 expression in relation to BRAF mutation, CpG island methylation and colorectal continuum in serrated lesions.	J Pathology	In press		2014
安井寛，今井浩三	がん免疫応答の制御：抗がん細胞抗体、その開発のあゆみとがん抗体療法の新たな可能性	実験医学	31(12)	121-127	2013

春日雅人, 植木浩二郎, 田嶼尚子, 野田光彦, 大橋健, 能登洋, 後藤温, 小川渉, 堺隆一, 津金昌一郎, 浜島信之, 中釜斉, 田島和雄, 宮園浩平, 今井浩三	糖尿病と癌に関する委員会報告	糖尿病	56(6)	374-390	2013
安井寛, 今井浩三	バイオ医薬品とＤＤＳ　特集「ＤＤＳ技術の進歩と医療応用」	メディカル・サイエンス・ダイジェスト	40(2)	15-18	2014
Saito T, Yano F, Mori D, Ohba S, Hojo H, Otsu M, Eto K, Nakauchi H, Tanaka S, Chung UI, Kawaguchi H	Generation of Col2a1-EGFP iPS cells for monitoring chondrogenic differentiation.	PLoS One.	8	e74137	2013
Razak SR, Ueno K, Takayama N, Nariai N, Nagasaki M, Saito R, Koso H, Lai CY, Murakami M, Tsuji K, Michiue T, Nakauchi H, Otsu M, Watanabe S.	Profiling of microRNA in human and mouse ES and iPS cells reveals overlapping but distinct microRNA expression patterns.	PLoS One.	8	e73532	2013
Hirata S, Takayama N, Jono-Ohnishi R, Endo H, Nakamura S, Dohda T, Nishi M, Hamazaki Y, Ishii E, Kaneko S, Otsu M, Nakauchi H, Kunishima S, Eto K.	Congenital amegakaryocytic thrombocytopenia iPS cells exhibit defective MPL-mediated signaling.	J Clin Invest.	123	3802-14	2013
Suzuki N, Yamazaki S, Yamaguchi T, Okabe M, Masaki H, Takaki S, Otsu M, Nakauchi H.	Generation of engraftable hematopoietic stem cells from induced pluripotent stem cells by way of teratoma formation.	Mol Ther.	21	1424-31	2013
He H. Nagamura-Inoue T., Tsunoda H., Yuzawa M., Yamamoto Y., Yorozu P., Agata H., Tojo A.	Stage-Specific Embryonic Antigen 4 in Wharton's Jelly-derived mesenchymal stem cells is not a marker for proliferation and multipotency.	Tissue Engineering, Part A			印刷中

He H, Tojo A et al.	Stage-Specific Embryonic Antigen 4 is not a marker for proliferation and pluripotency in Wharton's Jelly-derived mesenchymal stem cells.	Tissue Engineering Part A.	20 (7-8)	1314-24	2014
Yokoyama K, Tojo A, et al.	*In vivo* leukemogenic potential of an interleukin-7 receptor-α mutant in hematopoietic stem/progenitor cells.	Blood	22 (26)	4259-63	2013
Tomokuni A Tojo A, et al.	Effect of *in vivo* administration of reprogramming factors in the mouse liver.	Oncology Letters	6 (2)	323-8	2013
Okuyama K, Tojo A, et al.	miR-126-mediated control of cell fate in B cell-myeloid progenitors as a potential alternative to transcriptional factors.	Proceedings of the National Academy of Sciences USA	110 (33)	13410-5	2013
Kobayashi S, Tojo A, et al.	The CD3 versus CD7 plot in multicolor flow cytometry reflects progression of disease stage in patients infected with HTLV-I.	PLoS One.	8 (1)	e53728	2013
Morimoto A, Tojo A, et al.	Therapeutic outcome of multifocal Langerhans cell histiocytosis in adults treated with the Special C regimen formulated by the Japan LCH Study Group.	International Journal of Hematology	97 (1)	103-8	2013
Iida, A. et al.	Jmjd3 is required for the development of subsets of retinal bipolar cells	Proc.Natl. Acad. Sci., USA	111	3751-3756	2014
Koso, H. et al.	Transposon mutagenesis identifies Foxr2 as a putative oncogene in medulloblastoma	Can Res	74	2351-2361	2014

Mochizuki, Y. et al.	Use of cell type-specific transcriptome to identify genes specifically involved in Müller glia differentiation during retinal development	Dev Neurobiol	Nov4	in press	2013
Usui, A. et al.	The early retinal progenitor-expressed gene Sox11 regulates the timing of the differentiation of retinal cells	Developmen t	140	740-75 0	2013
Okada, H. et al.	Robust long-term transduction of common marmoset neuromuscular tissue with rAAV1 and rAAV9	Molecular Therapy - Nucleic Acids	2	e95	2013
Iwagawa, T. et al.	(2013) Enhancer/promoter activities of the long/middle wavelength-sensitive opsins of vertebrates mediated by thyroid hormone receptor β2 and COUP-TFII	Plos One	8	e7206 5	2013
Siti Razila Abdul Razak et al.	Profiling of MicroRNA in Human and Mouse ES and iPS Cells Reveals Overlapping but Distinct MicroRNA Expression Patterns.	Plos One	8(9)	e7353 2	2013
Komori T., Tanaka M., Senba E., Miyajima A. and Morikawa Y	Lack of Oncostatin M receptor β leads to adipose tissue inflammation and insulin resistance by switching macrophage phenotype.	J. Biol. Chem.	288	21861-21875,	2013
Miyaoka Y. and Miyajima A.	To divide or not to divide: revisiting liver regeneration.	Cell Division	8	8	2013

Taguchi K, Hirano I, Itoh T, Tanaka M, Miyajima A, Suzuki A, Motohashi H, and Yamamoto M	Nrf2 enhances cholangiocyte expansion in Pten-deficient livers	Mol. Cell. Biol.	34	900-91	2014
Itoh T. and Miyajima A.	Cellular Basis of Liver Regeneration.	Hepatology	59	1617-1626	2014
Yamauchi H, Motomura N, Chung UI, Sata M, Takai D, Saito A, Ono M, Takamoto S	Growth- associated hyperphosphatemia in young recipients accelerates aortic allograft calcification in a rat model.	J Thorac Cardiovasc Surg	145	522-30	2013
Umeki A, Nishimura T, Ando M, Takewa Y, Yamazaki K, Kyo S, Ono M, Tsukiya T, Mizuno T, Taenaka Y, Tatsumi E	Change of Coronary Flow by Continuous-Flow Left Ventricular Assist Device With Cardiac Beat Synchronizing System (Native Heart Load Control System) in Acute Ischemic Heart Failure Model.	Circ J	77	995-1000	2013
Umeki A, Nishimura T, Takewa Y, Ando M, Arakawa M, Kishimoto Y, Tsukiya T, Mizuno T, Kyo S, Ono M, Taenaka Y, Tatsumi E	Change in myocardial oxygen consumption employing continuous-flow LVAD with cardiac beat synchronizing system in acute ischemic heart failure models.	J Artif Organs	16	119-128	2013
Ando T, Kawashima D, Kim H, Joung S, Liao H, Kobayashi E, Gojo S, Kyo S, Ono M, Sakuma I	Direct minimal-invasive intraoperative electrophysiological mapping of the heart.	Minim Invasive Ther Allied Technol	22	372-80	2013
Ono M, Nishimura T, Kinoshita O, Shiga T, Kinugawa K , Nagai R, Kyo S	Improved survival in patients with continuous-flow ventricular assist device for bridge to heart transplantation.	Transplant Proc	45	2017-8	2013

Kimura M, Kinoshita O, Nishimura T, Imamura T, Shiga T, Kashiwa K, Kinugawa K, Kyo S, Ono M	Successful weaning from the DuraHeart with a low left ventricular ejection fraction.	J Artif Organs	16	504-7	2013
Inoue T, Kitamura T, Torii S, Hanayama N, Oka N, Itatani K, Tomoyasu T, Irisawa Y, Shibata M, Hayashi H, Ono M, Miyaji K	Five-week use of a monopivot centrifugal blood pump as a right ventricular assist device in severe dilated cardiomyopathy.	J Artif Organs	17	95-98	2014
Imamura T, Kinugawa K, Hatano M, Fujino T, Muraoka H, Inaba T, Maki H, Kagami Y, Endo M, Kinoshita O, Nawata K, Kyo S, Ono M	Preoperative beta-blocker treatment is a key for deciding left ventricular assist device implantation strategy as a bridge to recovery.	J Artif Organs	17	23-32	2014

IV. 研究成果の刊行物・別刷

(主なもの)

ARTICLE

doi:10.1038/nature12656

A small-molecule AdipoR agonist for type 2 diabetes and short life in obesity

Miki Okada-Iwabu[1,2,3]*, Toshimasa Yamauchi[1,2,3]*, Masato Iwabu[1,2]*, Teruki Honma[4], Ken-ichi Hamagami[1], Koichi Matsuda[1], Mamiko Yamaguchi[1], Hiroaki Tanabe[4], Tomomi Kimura-Someya[4], Mikako Shirouzu[4], Hitomi Ogata[5], Kumpei Tokuyama[5], Kohjiro Ueki[1], Tetsuo Nagano[6], Akiko Tanaka[4,6], Shigeyuki Yokoyama[4,7] & Takashi Kadowaki[1,2,3]

Adiponectin secreted from adipocytes binds to adiponectin receptors AdipoR1 and AdipoR2, and exerts antidiabetic effects via activation of AMPK and PPAR-α pathways, respectively. Levels of adiponectin in plasma are reduced in obesity, which causes insulin resistance and type 2 diabetes. Thus, orally active small molecules that bind to and activate AdipoR1 and AdipoR2 could ameliorate obesity-related diseases such as type 2 diabetes. Here we report the identification of orally active synthetic small-molecule AdipoR agonists. One of these compounds, AdipoR agonist (AdipoRon), bound to both AdipoR1 and AdipoR2 *in vitro*. AdipoRon showed very similar effects to adiponectin in muscle and liver, such as activation of AMPK and PPAR-α pathways, and ameliorated insulin resistance and glucose intolerance in mice fed a high-fat diet, which was completely obliterated in AdipoR1 and AdipoR2 double-knockout mice. Moreover, AdipoRon ameliorated diabetes of genetically obese rodent model *db/db* mice, and prolonged the shortened lifespan of *db/db* mice on a high-fat diet. Thus, orally active AdipoR agonists such as AdipoRon are a promising therapeutic approach for the treatment of obesity-related diseases such as type 2 diabetes.

The number of overweight individuals worldwide has grown markedly, leading to an escalation of obesity-related health problems associated with increased morbidity and mortality. Insulin resistance is a common feature of obesity and predisposes the affected individuals to a variety of pathologies, including type 2 diabetes and cardiovascular diseases. Although considerable progress has been made in understanding the molecular mechanisms underlying insulin resistance and type 2 diabetes, their satisfactory treatment modalities remain limited[1–4].

Adiponectin (*Adipoq*)[5–8] is an antidiabetic and antiatherogenic adipokine. Plasma adiponectin levels are decreased in obesity, insulin resistance and type 2 diabetes[9]. Replenishment of adiponectin has been shown to ameliorate insulin resistance and glucose intolerance in mice[10–12]. This insulin sensitizing effect of adiponectin seems to be mediated, at least in part, by an increase in fatty-acid oxidation via activation of AMP-activated protein kinase (AMPK)[13–15] and also via peroxisome proliferator-activated receptor (PPAR)-α[16,17].

We previously reported the expression cloning of complementary DNA encoding adiponectin receptors 1 and 2 (*Adipor1* and *Adipor2*)[18]. AdipoR1 and AdipoR2 are predicted to contain seven-transmembrane domains[18], but to be structurally and functionally distinct from G-protein-coupled receptors[19]. AdipoR1 and AdipoR2 serve as the major receptors for adiponectin *in vivo*, with AdipoR1 activating the AMPK pathways and AdipoR2 activating the PPAR-α pathways[20].

In skeletal muscle[21], AdipoR1 is predominantly expressed and activates AMPK[22] and PPAR-γ coactivator (PGC)-1α (ref. 23) as well as Ca^{2+} signalling pathways, which have also been shown to be activated by exercise[24,25]. Exercise has been reported to have beneficial effects on obesity-related diseases such as type 2 diabetes, and could contribute to healthy longevity[26]. Liver expresses AdipoR1 and AdipoR2, both of which have roles in the regulation of glucose and lipid metabolism, inflammation, and oxidative stress *in vivo*[20]. Here we report the discovery of an orally active synthetic small molecule that binds to and activates both AdipoR1 and AdipoR2, ameliorates insulin resistance and type 2 diabetes, and prolongs the shortened lifespan of *db/db* mice.

Identification of small-molecule agonists of AdipoR

To identify orally active compounds that could bind to and activate AdipoR, we screened a number of small molecules in the chemical library at Open Innovation Center for Drug Discovery, The University of Tokyo[27]. We performed functional assays to determine the ability of small molecules to activate AMPK (Extended Data Table 1 and Extended Data Fig. 1) and to ascertain the dependency of small molecules on AdipoR in C2C12 myotubes by testing the effects of suppression of AdipoR expression by specific short interfering RNA (siRNA) on phosphorylation of AMPK stimulated with each compound (Extended Data Table 2 and Extended Data Fig. 2). We named one of these hits AdipoR agonist (AdipoRon; Fig. 1a). We also used compounds 112254 and 165073 in some of the experiments as another hit and a non-hit, respectively (Extended Data Tables 1 and 2 and Extended Data Figs 1 and 2).

The treatment of C2C12 myotubes with AdipoRon caused an increase in the phosphorylation of Thr 172 in the α-subunit of AMPK (αAMPK)[28]. AdipoRon at concentrations of 5–50 μM increased AMPK phosphorylation in a dose-dependent manner to almost the same extent as did adiponectin (Fig. 1b, c) without mitochondrial complex I inhibition (Extended Data Fig. 3a). Suppression of AdipoR1 by specific siRNA (Extended Data Fig. 3b, c) greatly reduced the increase in AMPK phosphorylation induced by AdipoRon (Fig. 1c), indicating that AdipoRon increased AMPK phosphorylation via AdipoR1. Compound number 112254 (another hit) also significantly increased phosphorylation of

[1]Department of Diabetes and Metabolic Diseases, Graduate School of Medicine, The University of Tokyo, Tokyo 113-0033, Japan. [2]Department of Integrated Molecular Science on Metabolic Diseases, 22nd Century Medical and Research Center, The University of Tokyo, Tokyo 113-0033, Japan. [3]Department of Molecular Medicinal Sciences on Metabolic Regulation, 22nd Century Medical and Research Center, The University of Tokyo, Tokyo 113-0033, Japan. [4]RIKEN Systems and Structural Biology Center, Tsurumi, Yokohama 230-0045, Japan. [5]Graduate School of Comprehensive Human Sciences, University of Tsukuba, Tsukuba 305-8577, Japan. [6]Open Innovation Center for Drug Discovery, The University of Tokyo, 7-3-1 Hongo, Bunkyo-ku, Tokyo 113-0033, Japan. [7]Graduate School of Science, The University of Tokyo, Bunkyo-ku, Tokyo 113-0033, Japan.
*These authors contributed equally to this work.

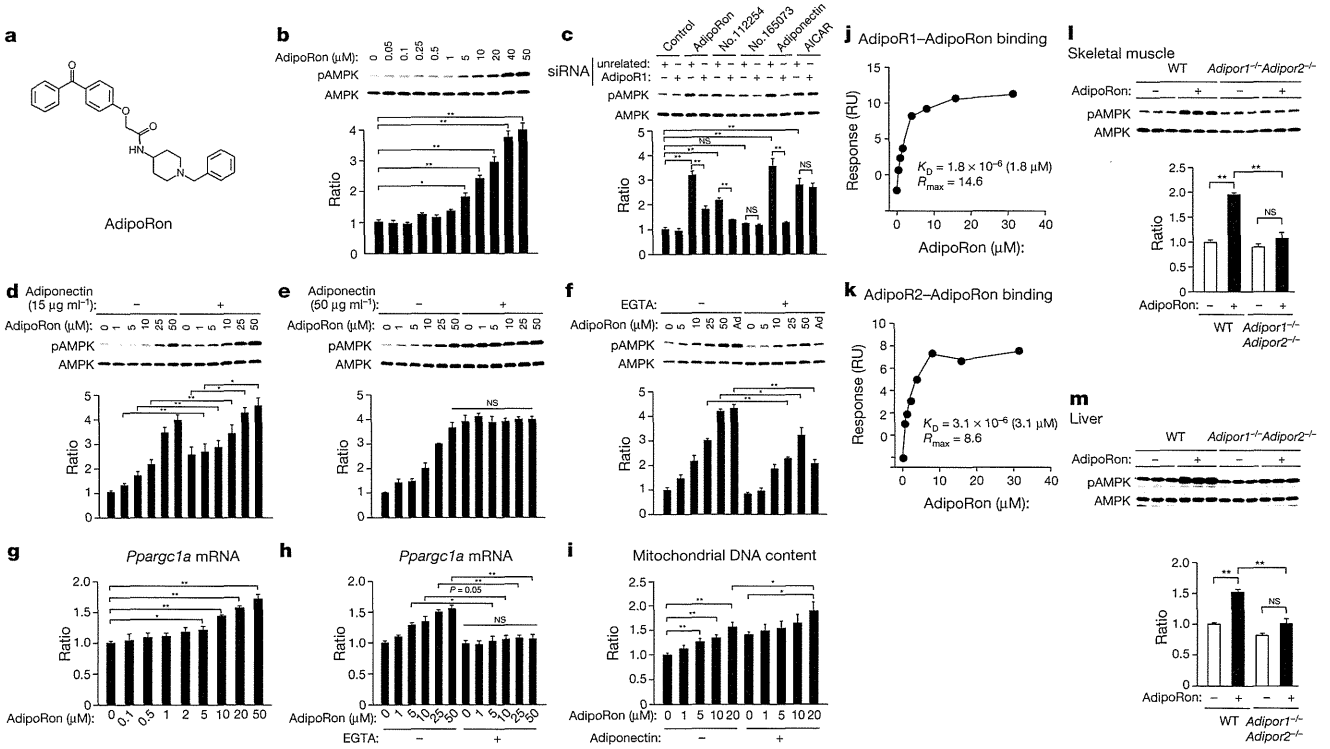

Figure 1 | Small-molecule AdipoR agonist AdipoRon binds to both AdipoR1 and AdipoR2, and increases AMPK activation, PGC-1α expression and mitochondrial biogenesis in C2C12 myotubes. **a**, Chemical structure of AdipoRon. **b–i**, **l**, **m**, Phosphorylation and amount of AMPK (**b–f**, **l**, **m**), *Ppargc1a* mRNA levels (**g**, **h**), and mitochondrial content as assessed by mitochondrial DNA copy number (**i**), in C2C12 myotubes after myogenic differentiation (**b–i**), in skeletal muscle (**l**) or in liver (**m**) from wild-type (WT) or *Adipor1*$^{-/-}$ *Adipor2*$^{-/-}$ double-knockout mice, treated with indicated concentrations of AdipoRon (**b**, **d–i**) or adiponectin (**d**, 15 μg ml^{-1}; **e**, 50 μg ml^{-1}; **i**, 10 μg ml^{-1}), for 5 min (**b**, **d–f**), 1.5 h (**g**, **h**) and 48 h (**i**), with or without EGTA (**f**, **h**), 25 μM AdipoRon, compound 112254 and 165073, 30 μg ml^{-1} adiponectin for 5 min or 1 mM AICAR for 1 h and transfected with or without the indicated siRNA duplex (**c**), or AdipoRon (**l**, **m**). **j**, **k**, Surface plasmon resonance measuring AdipoRon binding to AdipoR1 and AdipoR2. AdipoR1 and AdipoR2 were immobilized onto a sensor chip SA. Binding analyses were performed using a range of AdipoRon concentrations (0.49–31.25 μM). All values are presented as mean ± s.e.m. **b**, **c**, **e–I**, $n = 4$ each; **d**, **l**, **m**, $n = 3$ each; $^{*}P < 0.05$ and $^{**}P < 0.01$ compared to control or unrelated siRNA or as indicated. NS, not significant.

AMPK via AdipoR1, albeit less potently, and compound 165073 (a non-hit) failed to increase phosphorylation of AMPK (Fig. 1c).

In the presence or absence of the submaximal concentration of adiponectin (15 μg ml^{-1}), AdipoRon increased AMPK phosphorylation in a dose-dependent manner (Fig. 1d), whereas AdipoRon did not increase nor decrease AMPK phosphorylation in the presence of the maximal concentration of adiponectin (50 μg ml^{-1}) (Fig. 1e). These data suggested that AdipoRon replenished AMPK phosphorylation stimulated by adiponectin.

EGTA partially suppressed the AdipoRon-induced increase in AMPK phosphorylation in C2C12 myotubes (Fig. 1f), indicating that extracellular free Ca^{2+} is required for full AMPK phosphorylation stimulated with AdipoRon, like adiponectin[21]. Moreover, AdipoRon increased PGC-1α (*Ppargc1a*) expression (Fig. 1g, h) and mitochondrial DNA content (Fig. 1i) in a dose-dependent manner. Furthermore, EGTA effectively and almost completely abolished increased *Ppargc1a* expression stimulated with AdipoRon in C2C12 myotubes (Fig. 1h), consistent with the report that increased PGC-1α expression mediated by adiponectin is dependent on Ca^{2+} signalling[21].

By using surface plasmon resonance, AdipoRon bound to both AdipoR1 and AdipoR2 (dissociation constant (K_d) of 1.8 and 3.1 μM; R_{max} of 14.6 and 8.6 resonance units (RU), respectively) in a saturable manner (Fig. 1j, k). We also performed radioactive binding and Scatchard analysis and verified the specific binding of AdipoRon to AdipoR1 and AdipoR2 (Extended Data Fig. 4).

Intravenous injection of AdipoRon (50 mg kg^{-1} body weight) significantly induced phosphorylation of AMPK in skeletal muscle and liver of wild-type mice but not *Adipor1*$^{-/-}$ *Adipor2*$^{-/-}$ double-knockout mice (Fig. 1l, m), indicating that AdipoRon could activate AMPK in skeletal muscle and liver via AdipoR1 and AdipoR2.

AdipoRon ameliorates diabetes via AdipoR

To clarify whether orally administered small-molecule AdipoR agonist AdipoRon would exhibit a pharmacokinetic profile suitable for *in vivo* evaluation in the mouse, we measured plasma concentrations of AdipoRon in C57BL/6 wild-type mice after oral administration of 50 mg kg^{-1} of AdipoRon, and found that the maximal concentration (C_{max}) of AdipoRon was 11.8 μM (Fig. 2a and Extended Data Fig. 5a).

To test the therapeutic potential of a small-molecule AdipoR agonist to treat insulin resistance and diabetes, the effects of orally administered AdipoRon were examined in high-fat-diet-induced obese mice. Oral administration of AdipoRon (50 mg kg^{-1} body weight) for 10 days did not significantly affect body weight (Fig. 2b) nor food intake (Fig. 2c) in mice on a high-fat diet, but it did significantly reduce fasting plasma glucose and insulin levels as well as glucose and insulin responses during oral glucose tolerance tests in wild-type mice treated with AdipoRon (Fig. 2d and Extended Data Fig. 5b, c). The decrease in glucose levels in the face of reduced plasma insulin levels indicates improved insulin sensitivity (Fig. 2d, f and Extended Data Fig. 5d, e). Notably, treatment of *Adipor1*$^{-/-}$ *Adipor2*$^{-/-}$ double-knockout mice with AdipoRon failed to ameliorate high-fat-diet-induced hyperglycaemia and hyperinsulinaemia (Fig. 2e, f and Extended Data Fig. 5f–i).

The glucose-lowering effect of exogenous insulin was also greater in AdipoRon-treated wild-type mice than in vehicle-treated control

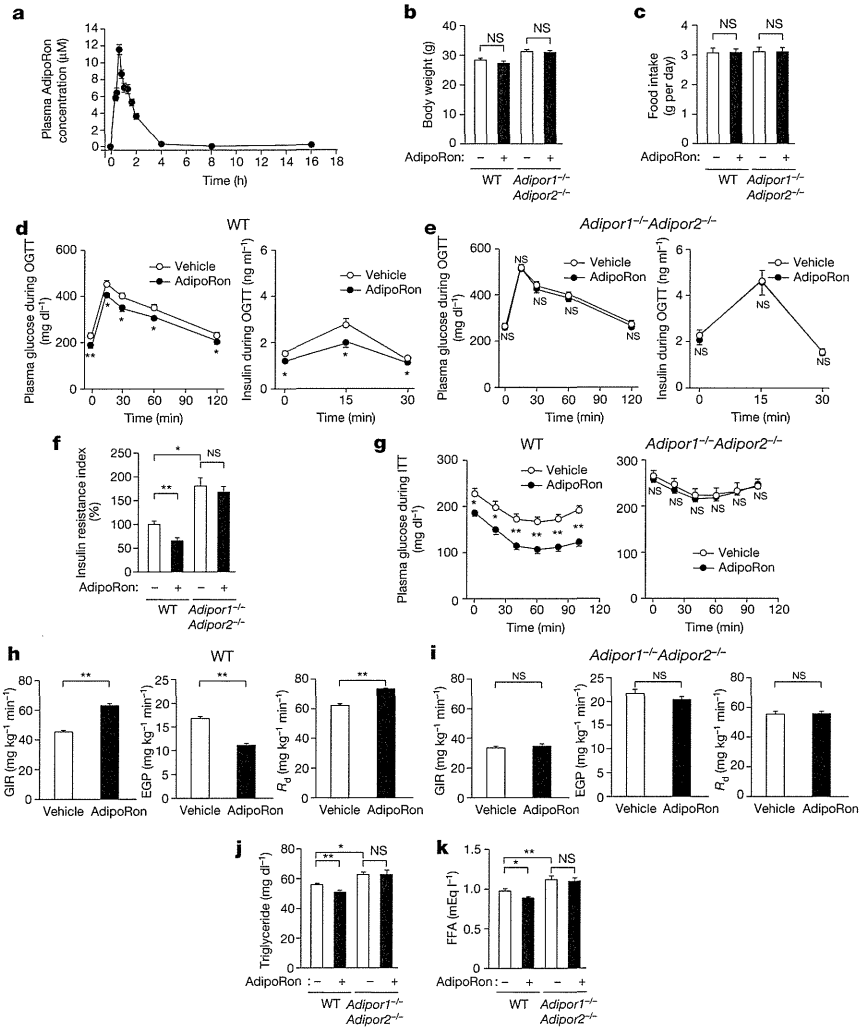

Figure 2 | AdipoRon improved insulin resistance, glucose intolerance and dyslipidaemia via AdipoR. **a**–**g**, Plasma AdipoRon concentrations (**a**), body weight (**b**), food intake (**c**), plasma glucose (**d**, **e**, **g**), plasma insulin (**d**, **e**) and insulin resistance index (**f**) during oral glucose tolerance test (OGTT) (1.0 g glucose per kg body weight) (**d**, **e**) or during insulin tolerance test (ITT) (0.5 U insulin per kg body weight) (**g**) in wild-type (WT) and *Adipor1*$^{-/-}$ *Adipor2*$^{-/-}$ double-knockout mice, treated with or without AdipoRon (50 mg per kg body weight). **h**, **i**, Glucose infusion rate (GIR), endogenous glucose production (EGP) and rates of glucose disposal (R_d) during hyperinsulinaemic euglycaemic clamp study in wild-type and *Adipor1*$^{-/-}$ *Adipor2*$^{-/-}$ double-knockout mice, treated with or without AdipoRon (50 mg per kg body weight). **j**, **k**, Plasma triglyceride (**j**) and free fatty acid (FFA) (**k**) in wild-type and *Adipor1*$^{-/-}$ *Adipor2*$^{-/-}$ double-knockout mice, treated with or without AdipoRon (50 mg per kg body weight). All values are presented as mean ± s.e.m. **a**, $n = 12$–32; **b**–**g**, **j**, **k**, $n = 10$ each; **h**, **i**, $n = 5$ each; $^{*}P < 0.05$ and $^{**}P < 0.01$ compared to control or as indicated. NS, not significant.

wild-type mice (Fig. 2g, left, and Extended Data Fig. 5j, k), which was not observed in *Adipor1*$^{-/-}$ *Adipor2*$^{-/-}$ double-knockout mice (Fig. 2g, right, and Extended Data Fig. 5l, m).

We examined whether a similar chemical analogue of AdipoRon that could activate AMPK via AdipoR would have an antidiabetic effect. Consistent with this, we observed that another similar chemical analogue of AdipoRon, compound 112254 (Extended Data Fig. 6a), could activate AMPK (Fig. 1c) and at the same time ameliorate both glucose intolerance and insulin resistance (Extended Data Fig. 6c–f). Conversely, we observed that another compound, 165073 (Extended Data Fig. 6b), could not activate AMPK (Fig. 1c), ameliorate glucose intolerance, nor ameliorate insulin resistance (Extended Data Fig. 6g–j).

We performed hyperinsulinaemic euglycaemic clamps in mice on a high-fat diet after 10 days of treatment. The glucose infusion rate was significantly increased (Fig. 2h, left), the endogenous glucose production was significantly suppressed (Fig. 2h, middle), and the glucose disposal rate was significantly increased (Fig. 2h, right) in AdipoRon-treated wild-type mice. None of these parameters was improved on AdipoRon treatment in *Adipor1*$^{-/-}$ *Adipor2*$^{-/-}$ double-knockout mice (Fig. 2i).

We next examined the effects of AdipoRon on lipid metabolism. Treatment with AdipoRon for 10 days reduced plasma concentrations of triglycerides and free fatty acid (FFA) in wild-type mice fed a high-fat diet (Fig. 2j, k), an effect that was not observed in *Adipor1*$^{-/-}$ *Adipor2*$^{-/-}$ double-knockout mice (Fig. 2j, k).

AdipoRon activates AdipoR1–AMPK–PGC-1α pathways

In skeletal muscle of wild-type mice, AdipoRon increased the expression of genes involved in mitochondrial biogenesis such as *Ppargc1a* and oestrogen-related receptor-α (*Esrra*)[29], mitochondrial DNA replication/translation such as mitochondrial transcription factor A (*Tfam*), and oxidative phosphorylation such as cytochrome *c* oxidase subunit II (*mt-Co2*) (Fig. 3a). AdipoRon also increased mitochondrial DNA content in the skeletal muscle of wild-type mice (Fig. 3b). These effects were completely obliterated in *Adipor1*$^{-/-}$ *Adipor2*$^{-/-}$ double-knockout mice (Fig. 3a, b).

AdipoRon increased the levels of oxidative, high endurance type I fibre[30] marker troponin I (slow) (*Tnni1*) in the skeletal muscle of wild-type mice (Fig. 3a) but not in *Adipor1*$^{-/-}$ *Adipor2*$^{-/-}$ double-knockout mice (Fig. 3a). We challenged mice fed a high-fat diet with involuntary physical exercise by treadmill running and then assessed muscle endurance. AdipoRon significantly increased exercise endurance in wild-type mice, but not in *Adipor1*$^{-/-}$ *Adipor2*$^{-/-}$ double-knockout mice (Fig. 3c) fed a high-fat diet.

We next examined the expression of metabolic genes and found that AdipoRon significantly increased the expression of genes involved in fatty-acid oxidation such as medium-chain acyl-CoA dehydrogenase (*Acadm*) (Fig. 3a), which was associated with decreased triglyceride content[31] (Extended Data Fig. 7a), in the skeletal muscle of wild-type mice but not of *Adipor1*$^{-/-}$ *Adipor2*$^{-/-}$ double-knockout mice fed a high-fat diet.

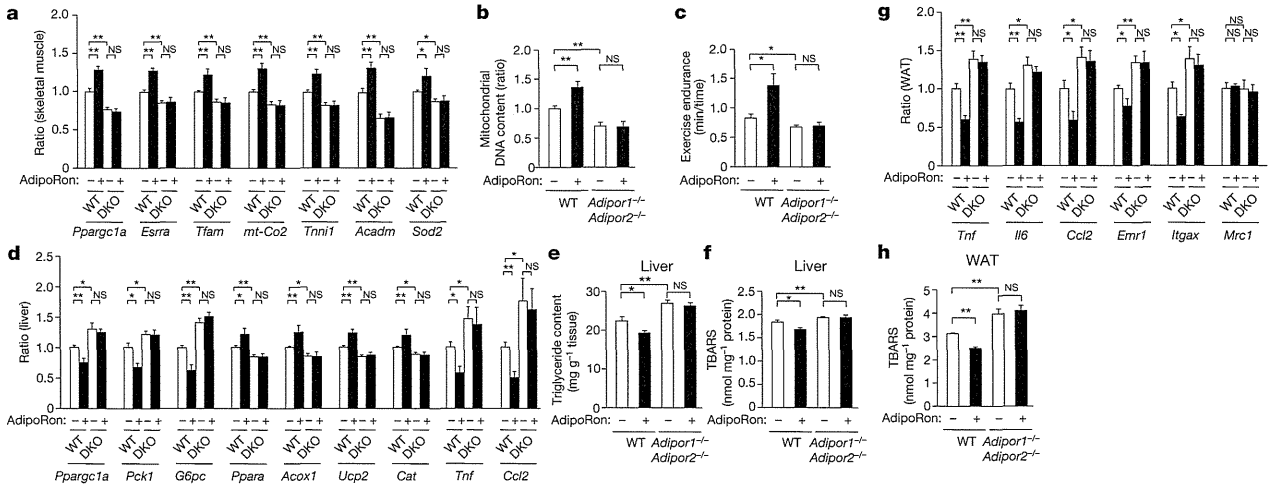

Figure 3 | AdipoRon increased mitochondria biogenesis in muscle, reduced tissue triglyceride content in liver and decreased oxidative stress and inflammation in liver and WAT. a–h, *Ppargc1a*, *Esrra*, *Tfam*, *mt-Co2*, *Tnni1*, *Acadm* and *Sod2* mRNA levels (**a**), mitochondrial content as assessed by mitochondrial DNA copy number (**b**) in skeletal muscle, exercise endurance (**c**), *Ppargc1a*, *Pck1*, *G6pc*, *Ppara*, *Acox1*, *Ucp2*, *Cat*, *Tnf* and *Ccl2* mRNA levels (**d**), tissue triglyceride content (**e**), TBARS (**f**) in liver and *Tnf*, *Il6*, *Ccl2*, *Emr1*, *Itgax* and *Mrc1* mRNA levels (**g**) and TBARS (**h**) in WAT, from wild-type and *Adipor1*$^{-/-}$*Adipor2*$^{-/-}$ double-knockout (DKO) mice treated with or without AdipoRon (50 mg per kg body weight). All values are presented as mean ± s.e.m. **a**, **b**, **d**–**h**, $n = 10$ each; **c**, $n = 5$ each; $^{*}P < 0.05$ and $^{**}P < 0.01$ compared to control or as indicated. NS, not significant.

AdipoRon significantly increased the expression levels for oxidative stress-detoxifying genes such as manganese superoxide dismutase (*Sod2*) (Fig. 3a), and decreased oxidative stress markers[32] such as thiobarbituric acid reactive substance (TBARS) (Extended Data Fig. 7b), in the skeletal muscle of wild-type mice but not of *Adipor1*$^{-/-}$ *Adipor2*$^{-/-}$ double-knockout mice fed a high-fat diet.

AdipoRon also activates AdipoR2–PPAR-α pathways

We examined whether AdipoRon could activate AdipoR1 and AdipoR2 pathways in the liver. The activation of AdipoR1–AMPK pathway in the liver has been reported to reduce the expression of genes involved in hepatic gluconeogenesis such as *Ppargc1a*, phosphoenolpyruvate carboxykinase 1 (*Pck1*)[20,33] and glucose-6-phosphatase (*G6pc*). As predicted by these earlier studies, we found that AdipoRon significantly decreased the expression of *Ppargc1a*, *Pck1* and *G6pc* in the liver of wild-type (Fig. 3d) but not of *Adipor1*$^{-/-}$ *Adipor2*$^{-/-}$ double-knockout mice (Fig. 3d) fed a high-fat diet.

Activation of AdipoR2 can increase PPAR-α levels and activate PPAR-α pathways, leading to increased fatty-acid oxidation and reduction of oxidative stress[20]. AdipoRon increased the expression levels of the gene encoding PPAR-α itself (*Ppara*) and its target genes[16], including genes involved in fatty-acid combustion such as acyl-CoA oxidase (*Acox1*), genes involved in energy dissipation such as uncoupling protein 2 (*Ucp2*), and genes encoding oxidative stress detoxifying enzymes such as catalase (*Cat*) in the liver of wild-type (Fig. 3d) but not of *Adipor1*$^{-/-}$ *Adipor2*$^{-/-}$ double-knockout mice (Fig. 3d) fed a high-fat diet. AdipoRon significantly reduced triglyceride content (Fig. 3e) and oxidative stress[32], as measured by TBARS (Fig. 3f), in the liver of wild-type mice but not of *Adipor1*$^{-/-}$ *Adipor2*$^{-/-}$ double-knockout mice (Fig. 3e, f) fed a high-fat diet.

Notably, orally administered AdipoRon reduced the expression levels of the genes encoding pro-inflammatory cytokines such as TNF-α (*Tnf*)[34] and MCP-1 (*Ccl2*) in the liver of wild-type mice (Fig. 3d) but not of *Adipor1*$^{-/-}$ *Adipor2*$^{-/-}$ double-knockout mice (Fig. 3d) fed a high-fat diet.

AdipoRon decreases inflammation

AdipoRon reduced the expression levels of genes encoding pro-inflammatory cytokines[35–37] such as *Tnf*, IL-6 (*Il6*) and *Ccl2* in the white adipose tissue (WAT) of wild-type mice but not of *Adipor1*$^{-/-}$ *Adipor2*$^{-/-}$ double-knockout mice fed a high-fat diet (Fig. 3g). Notably, AdipoRon reduced TBARS (Fig. 3h) and reduced levels of macrophage markers such as F4/80 (*Emr1*), and especially the levels of markers for classically activated M1 macrophages such as CD11c (*Itgax*)[38]—but not the levels of markers for the alternatively activated M2 macrophages such as CD206 (*Mrc1*)—in the WAT of wild-type mice fed a high-fat diet (Fig. 3g), whereas these changes were not observed in *Adipor1*$^{-/-}$ *Adipor2*$^{-/-}$ double-knockout mice (Fig. 3g, h).

AdipoRon ameliorates diabetes in *db/db* mice

We next studied the effects of AdipoRon (50 mg kg^{-1} body weight) in a genetically obese rodent model (*Lepr*$^{-/-}$ (also known as *db/db*) mice); *db/db* mice fed a normal chow diet exhibit decreased plasma adiponectin concentrations[6,10]. As was expected[13], intraperitoneal injection of adiponectin into *db/db* mice reduced plasma glucose levels (Fig. 4a, left and right panels). Interestingly, orally administered AdipoRon also significantly reduced plasma glucose levels as quickly and potently as did intraperitoneal adiponectin injection in *db/db* mice (Fig. 4a, middle and right panels).

Without affecting body weight, food intake, liver weight and WAT weight (Fig. 4b–e), orally administered AdipoRon for 2 weeks significantly ameliorated glucose intolerance, insulin resistance and dyslipidaemia in *db/db* mice fed a normal chow diet (Fig. 4f–i).

In the skeletal muscle of *db/db* mice fed a normal chow diet, AdipoRon significantly increased the expression levels of genes involved in mitochondrial biogenesis functions and DNA content (Fig. 5a, b), and also *Acadm* and *Sod2* (Fig. 5a), which were associated with decreased triglyceride content and TBARS (Fig. 5c, d), respectively. In the liver, AdipoRon significantly decreased the expression of *Ppargc1a*, *Pck1* and *G6pc* (Fig. 5e), increased the expression of *Ppara* and its target genes (Fig. 5e). Therefore, Adipron significantly reduced triglyceride content (Fig. 5f), oxidative stress (Fig. 5g) and reduced the expression levels of genes encoding pro-inflammatory cytokines (Fig. 5e). In the WAT, AdipoRon reduced the expression levels of genes encoding pro-inflammatory cytokines and macrophage markers, especially the levels of markers for classically activated M1 macrophages, but not the levels of markers for the alternatively activated M2 macrophages (Fig. 5h).

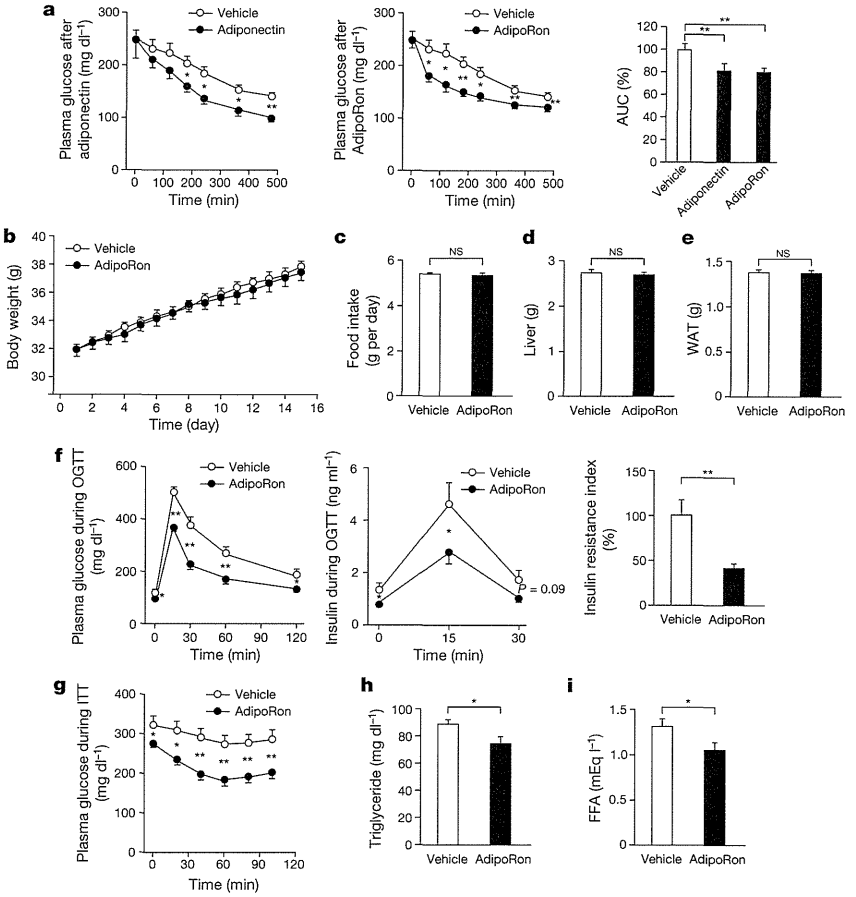

Figure 4 | AdipoRon ameliorated insulin resistance, diabetes and dyslipidaemia in *db/db* mice. **a**, Plasma glucose levels after intraperitoneal injection of adiponectin (30 μg per 10 g body weight) (left) or after oral administration of AdipoRon (50 mg per kg body weight) (middle). The area under the curve (AUC) of left and middle panels is shown on the right. **b–i**, Body weight (**b**), food intake (**c**), liver weight (**d**), WAT weight (**e**), plasma glucose (**f**, left, **g**), plasma insulin (**f**, middle) and insulin resistance index (**f**, right) during oral glucose tolerance test (OGTT) (1.0 g glucose per kg body weight) (**f**) or during insulin tolerance test (ITT) (0.75 U insulin per kg body weight) (**g**), plasma triglyceride (**h**) and free fatty acid (FFA) (**i**) in *db/db* mice under normal chow conditions, treated with or without AdipoRon (50 mg per kg body weight). All values are presented as mean ± s.e.m. **a**, $n = 6$-7; **b–i**, $n = 10$ each from 2–3 independent experiments, $^{*}P < 0.05$ and $^{**}P < 0.01$ compared to control or as indicated. NS, not significant.

AdipoRon prolonged the shortened lifespan

Notably, *Adipor1*$^{-/-}$ *Adipor2*$^{-/-}$ double-knockout mice showed a shortened lifespan as compared with wild-type mice under both normal chow diet and high-fat diet conditions (Fig. 6a, b). Because a high-fat diet has been reported to shorten lifespan[39], we examined whether orally administered AdipoR agonists could prolong the shortened lifespan on a high-fat diet. Lifespan of *db/db* mice on a high-fat diet was markedly shortened as compared with that on a normal chow diet. Surprisingly, AdipoRon significantly rescued the shortened lifespan of *db/db* mice on a high-fat diet (Fig. 6c).

The decreased effects of adiponectin in obesity have been reported to have causal roles in the development of obesity-related diseases such as diabetes[40] and cardiovascular diseases[41]. There are two strategies to reverse reduced adiponectin effects. One is to increase the levels of adiponectin itself, such as through the injection of adiponectin. However, there are many difficulties associated with adiponectin injection, such as very high plasma concentrations of adiponectin and high-molecular-weight adiponectin multimers as highest activity form[42].

An alternative strategy is to activate adiponectin receptors. Both AdipoR1 and AdipoR2 have roles in the regulation of glucose and lipid metabolism, inflammation, and oxidative stress *in vivo*[20]. Therefore, the development of orally active small-molecule agonists for both AdipoR1 and AdipoR2 has long been sought. Here, we have identified and characterized an orally active synthetic small molecule that binds to and activates AdipoR1 and AdipoR2. So far, the top four hits obtained through the screening campaign have common structural motifs (Extended Data Fig. 8) (see additional results and discussion in Supplementary Information).

One of these small molecules, AdipoRon, binds to both AdipoR1 and AdipoR2 *in vitro* (K_d 1.8 and 3.1 μM; R_{max} 14.6 and 8.6 RU, respectively), activates AMPK, and increases PGC-1α levels and mitochondrial DNA content in myotubes (Fig. 1). When AdipoRon was administered orally to mice (50 mg per kg body weight), it was confirmed that the concentrations of AdipoRon in plasma (C_{max} of 11.8 μM) reached levels greater than the K_d values (AdipoR1, 1.8 μM; AdipoR2, 3.1 μM) (Fig. 2a). After the concentration reached the maximum as shown in Fig. 2a, the effect reached the maximum (Extended Data Fig. 5n), and the effect lasted for at least 8 h. Orally administered AdipoRon ameliorated insulin resistance, glucose intolerance and dyslipidaemia in mice fed a high-fat diet (Fig. 2d–k). Notably, these beneficial effects were completely obliterated in *Adipor1*$^{-/-}$ *Adipor2*$^{-/-}$ double-knockout mice (Fig. 2d–k) but partially preserved in *Adipor1*$^{-/-}$ or *Adipor2*$^{-/-}$ single-knockout mice (Extended Data Fig. 7c-g), indicating that AdipoRon works through both AdipoR1 and AdipoR2 *in vivo*.

Adiponectin ameliorated insulin resistance and glucose intolerance via multiple mechanisms including activation of AMPK, decreased oxidative stress, decreased tissue triglyceride content and suppression of inflammation[13,14]. AdipoRon exerted multiple effects very similar to those of adiponectin described above *in vivo*, and ameliorated insulin resistance and glucose intolerance via AdipoR1 and AdipoR2 in obese diabetic mice on a high-fat diet (Fig. 3).

In this study, we show that in skeletal muscle of obese diabetic mice such as wild-type mice on a high-fat diet (Fig. 3) and *db/db* mice (Figs 4 and 5), AdipoR1 and AdipoR2 agonists such as AdipoRon increase mitochondrial biogenesis, which was associated with increased

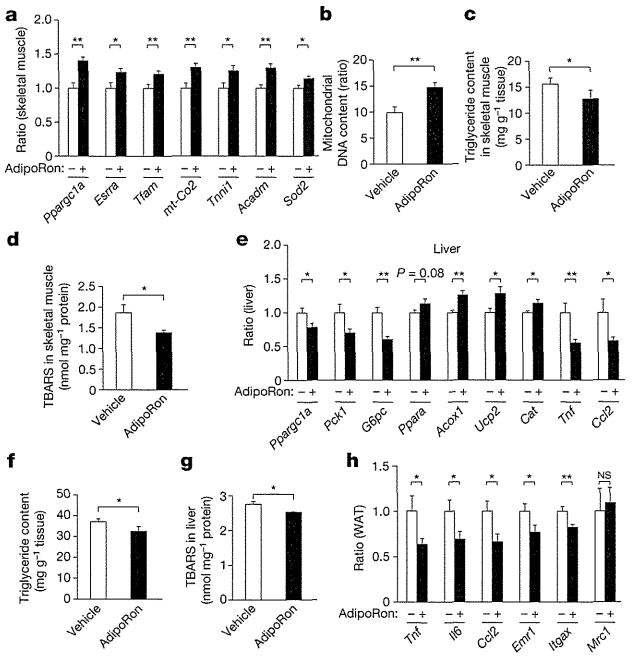

Figure 5 | AdipoRon increased mitochondria biogenesis in muscle, reduced tissue triglyceride content and oxidative stress in muscle and liver, and decreased inflammation in liver and WAT of *db/db* mice. **a**–**h**, *Ppargc1a*, *Esrra*, *Tfam*, *mt-Co2*, *Tnni1*, *Acadm* and *Sod2* mRNA levels (**a**), and mitochondrial content as assessed by mitochondrial DNA copy number (**b**), tissue triglyceride content (**c**) and TBARS (**d**) in skeletal muscle, *Ppargc1a*, *Pck1*, *G6pc*, *Ppara*, *Acox1*, *Ucp2*, *Cat*, *Tnf* and *Ccl2* mRNA levels (**e**), tissue triglyceride content (**f**) and TBARS (**g**) in liver, and *Tnf*, *Il6*, *Ccl2*, *Emr1*, *Itgax* and *Mrc1* mRNA levels (**h**) in WAT from *db/db* mice on a normal chow diet, treated with or without AdipoRon (50 mg per kg body weight). All values are presented as mean ± s.e.m. $n = 10$, $^{*}P < 0.05$ and $^{**}P < 0.01$ compared to control or as indicated. NS, not significant.

exercise endurance, and at the same time increase expression levels of genes involved in fatty-acid combustion, oxidative phosphorylation and reduction of oxidative stress (Figs 3, 5 and 6d). In liver, AdipoRon suppresses the expression of genes involved in gluconeogenesis, increases expression of PPAR-α target genes involved in fatty-acid combustion, and reduces oxidative stress (Figs 3, 5 and 6d). In WAT, AdipoRon reduces oxidative stress and pro-inflammatory cytokines, and the accumulation of M1 macrophages (Figs 3, 5 and 6d). Importantly, these effects resulted in reduced tissue triglyceride content in liver and muscle, and oxidative stress in liver, muscle and WAT, and decreased inflammation in liver and WAT (Figs 3–5 and 6d). These alterations collectively result in increased insulin sensitivity and glucose tolerance (Fig. 6d).

Therefore, we could expect AdipoRon to exert most, if not all, of the effects exerted by adiponectin, such as increased insulin sensitivity and glucose tolerance, as well as suppression of cardiovascular diseases and cancer, as previously reported[17,41,43]. Indeed, AdipoRon did prolong the shortened lifespan of obese diabetic mice (Fig. 6a–d).

Taken together, our findings show that the orally active small-molecule AdipoR agonist AdipoRon shifts the physiology of mice fed excess calorie towards that of mice fed a standard diet, modulates known longevity pathways, and improves health and prolongs lifespan. This study provides evidence that an orally available synthetic small-molecule AdipoR agonist at doses achievable *in vivo* can safely reduce many of the unhealthy and undesirable consequences of excess calorie intake and sedentary lifestyle, with an overall improvement in health and even lifespan, much like calorie restriction and exercise. Because virtually all current therapeutic modalities of type 2 diabetes require stringent adherence to diet and exercise and are associated with adverse effects such as hypoglycaemia and weight gain, AdipoRon provides a novel pre-emptive medicine and treatment modality. Orally active AdipoR agonists are a promising novel therapeutic approach for treating obesity-related disorders such as type 2 diabetes.

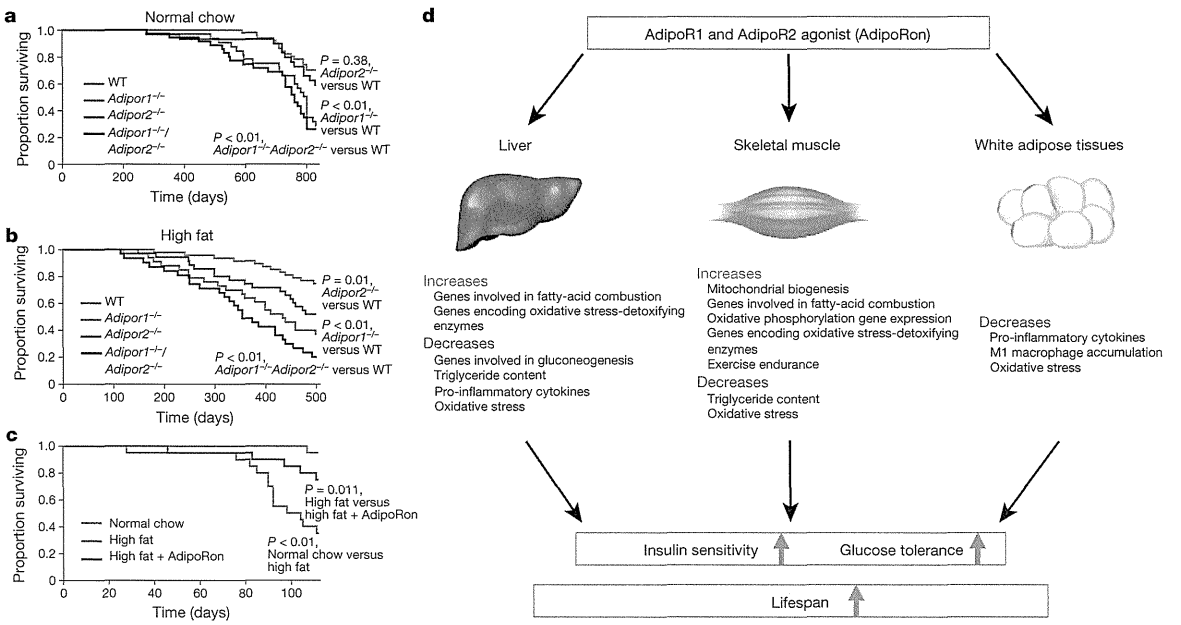

Figure 6 | AdipoRon increased insulin sensitivity and glucose tolerance, and at the same time contributed to longevity of obese diabetic mice. **a**–**c**, Kaplan–Meier survival curves for wild-type, *Adipor1*$^{-/-}$, *Adipor2*$^{-/-}$ and *Adipor1*$^{-/-}$ *Adipor2*$^{-/-}$ knockout mice on a normal chow diet (**a**) ($n = 50$, 32, 29 and 35, respectively) or high-fat diet (**b**) ($n = 47$, 33, 35 and 31, respectively), or for *db/db* mice treated with or without AdipoRon (30 mg per kg body weight) on a normal chow or high-fat diet ($n = 20$ each) (**c**). *P* values were derived from log-rank calculations. **d**, Scheme illustrating the mechanisms by which AdipoR1 and AdipoR2 agonist increases insulin sensitivity and glucose tolerance, and at the same time lifespan. (See also main text.)

METHODS SUMMARY

Mice. Mice were 6–10 weeks of age at the time of the experiment. The animal care and use procedures were approved by the Animal Care Committee of the University of Tokyo (see additional Methods in Supplementary Information).

Studies with C2C12 cells. Induction of myogenic differentiation was carried out according to a method described previously[21]. By day 5, the cells had differentiated into multinucleated contracting myotubes. C2C12 myotubes were used after myogenic differentiation in all experiments.

Survival. The wild-type, *Adipor1*$^{-/-}$, *Adipor2*$^{-/-}$, *Adipor1*$^{-/-}$ *Adipor2*$^{-/-}$ knockout mice and the *db/db* mice were maintained with food and water ad libitum. In these experiments, we used standard chow diet (CE-2, CLEA Japan Inc.) or high-fat diet 32 (CLEA Japan Inc.)[20]. For the experiment shown in Fig. 6a, b, wild-type ($n = 50$), *Adipor1*$^{-/-}$ ($n = 32$), *Adipor2*$^{-/-}$ ($n = 29$) and *Adipor1*$^{-/-}$ *Adipor2*$^{-/-}$ ($n = 35$) knockout mice fed a normal chow diet were used. For the experiment shown in Fig. 6b, wild-type ($n = 47$), *Adipor1*$^{-/-}$ ($n = 33$), *Adipor2*$^{-/-}$ ($n = 35$) and *Adipor1*$^{-/-}$ *Adipor2*$^{-/-}$ ($n = 31$) knockout mice on a high-fat diet were used. For the experiment shown in Fig. 6c, the *db/db* mice were randomly divided into three groups: a normal chow group (normal chow, $n = 20$), high-fat group (high fat, $n = 20$) and high-fat plus AdipoRon group (high fat + AdipoRon, $n = 20$), which were treated with AdipoRon at a daily dose of 30 mg kg^{-1} body weight. The survival rate was recorded daily. Survival curves were plotted using the Kaplan–Meier method.

Statistical analysis. Results are expressed as mean ± s.e.m. Differences between two groups were assessed using unpaired two-tailed *t*-tests. Data involving more than two groups were assessed by analysis of variance (ANOVA).

Online Content Any additional Methods, Extended Data display items and Source Data are available in the online version of the paper; references unique to these sections appear only in the online paper.

Received 6 June 2012; accepted 10 September 2013.
Published online 30 October 2013.

1. Gesta, S., Tseng, Y. H. & Kahn, C. R. Developmental origin of fat: tracking obesity to its source. *Cell* **131,** 242–256 (2007).
2. Olefsky, J. M. & Glass, C. K. Macrophages, inflammation, and insulin resistance. *Annu. Rev. Physiol.* **72,** 219–246 (2010).
3. Osler, M. E. & Zierath, J. R. Adenosine 5′-monophosphate-activated protein kinase regulation of fatty acid oxidation in skeletal muscle. *Endocrinology* **149,** 935–941 (2008).
4. LeRoith, D. & Accili, D. Mechanisms of disease: using genetically altered mice to study concepts of type 2 diabetes. *Nature Clin. Pract. Endocrinol. Metab.* **4,** 164–172 (2008).
5. Scherer, P. E., Williams, S., Fogliano, M., Baldini, G. & Lodish, H. F. A novel serum protein similar to C1q, produced exclusively in adipocytes. *J. Biol. Chem.* **270,** 26746–26749 (1995).
6. Hu, E., Liang, P. & Spiegelman, B. M. AdipoQ is a novel adipose-specific gene dysregulated in obesity. *J. Biol. Chem.* **271,** 10697–10703 (1996).
7. Maeda, K. *et al.* cDNA cloning and expression of a novel adipose specific collagen-like factor, apM1 (AdiPose most abundant gene transcript 1). *Biochem. Biophys. Res. Commun.* **221,** 286–289 (1996).
8. Nakano, Y., Tobe, T., Choi-Miura, N. H., Mazda, T. & Tomita, M. Isolation and characterization of GBP28, a novel gelatin-binding protein purified from human plasma. *J. Biochem.* **120,** 803–812 (1996).
9. Hotta, K. *et al.* Plasma concentrations of a novel, adipose-specific protein, adiponectin, in type 2 diabetic patients. *Arterioscler. Thromb. Vasc. Biol.* **20,** 1595–1599 (2000).
10. Yamauchi, T. *et al.* The fat-derived hormone adiponectin reverses insulin resistance associated with both lipoatrophy and obesity. *Nature Med.* **7,** 941–946 (2001).
11. Berg, A. H., Combs, T. P., Du, X., Brownlee, M. & Scherer, P. E. The adipocyte-secreted protein Acrp30 enhances hepatic insulin action. *Nature Med.* **7,** 947–953 (2001).
12. Fruebis, J. *et al.* Proteolytic cleavage product of 30-kDa adipocyte complement-related protein increases fatty acid oxidation in muscle and causes weight loss in mice. *Proc. Natl Acad. Sci. USA* **98,** 2005–2010 (2001).
13. Yamauchi, T. *et al.* Adiponectin stimulates glucose utilization and fatty-acid oxidation by activating AMP-activated protein kinase. *Nature Med.* **8,** 1288–1295 (2002).
14. Tomas, E. *et al.* Enhanced muscle fat oxidation and glucose transport by ACRP30 globular domain: acetyl-CoA carboxylase inhibition and AMP-activated protein kinase activation. *Proc. Natl Acad. Sci. USA* **99,** 16309–16313 (2002).
15. Kahn, B. B., Alquier, T., Carling, D. & Hardie, D. G. AMP-activated protein kinase: ancient energy gauge provides clues to modern understanding of metabolism. *Cell Metab.* **1,** 15–25 (2005).
16. Kersten, S., Desvergne, B. & Wahli, W. Roles of PPARs in health and disease. *Nature* **405,** 421–424 (2000).
17. Yamauchi, T. *et al.* Globular adiponectin protected ob/ob mice from diabetes and apoE deficient mice from atherosclerosis. *J. Biol. Chem.* **278,** 2461–2468 (2003).
18. Yamauchi, T. *et al.* Cloning of adiponectin receptors that mediate antidiabetic metabolic effects. *Nature* **423,** 762–769 (2003).
19. Wess, J. G-protein-coupled receptors: molecular mechanisms involved in receptor activation and selectivity of G-protein recognition. *FASEB J.* **11,** 346–354 (1997).
20. Yamauchi, T. *et al.* Targeted disruption of AdipoR1 and AdipoR2 causes abrogation of adiponectin binding and metabolic actions. *Nature Med.* **13,** 332–339 (2007).
21. Iwabu, M. *et al.* Adiponectin and AdipoR1 regulate PGC-1α and mitochondria by Ca^{2+} and AMPK/SIRT1. *Nature* **464,** 1313–1319 (2010).
22. Richter, E. A. & Ruderman, N. B. AMPK and the biochemistry of exercise: implications for human health and disease. *Biochem. J.* **418,** 261–275 (2009).
23. Wu, Z. *et al.* Mechanisms controlling mitochondrial biogenesis and respiration through the thermogenic coactivator PGC-1. *Cell* **98,** 115–124 (1999).
24. Handschin, C. & Spiegelman, B. M. The role of exercise and PGC1α in inflammation and chronic disease. *Nature* **454,** 463–469 (2008).
25. Cantó, C. *et al.* AMPK regulates energy expenditure by modulating NAD^+ metabolism and SIRT1 activity. *Nature* **458,** 1056–1060 (2009).
26. Paffenbarger, R. S. Jr *et al.* The association of changes in physical-activity level and other lifestyle characteristics with mortality among men. *N. Engl. J. Med.* **328,** 538–545 (1993).
27. Open Innovation Center for Drug Discovery. http://www.ocdd.u-tokyo.ac.jp/library_e.html (The University of Tokyo, 2012).
28. Hawley, S. A. *et al.* Characterization of the AMP-activated protein kinase kinase from rat liver and identification of threonine 172 as the major site at which it phosphorylates AMP-activated protein kinase. *J. Biol. Chem.* **271,** 27879–27887 (1996).
29. Mootha, V. K. *et al.* Errα and Gabpa/b specify PGC-1α-dependent oxidative phosphorylation gene expression that is altered in diabetic muscle. *Proc. Natl Acad. Sci. USA* **101,** 6570–6575 (2004).
30. Berchtold, M. W. *et al.* Calcium ion in skeletal muscle: its crucial role for muscle function, plasticity, and disease. *Physiol. Rev.* **80,** 1215–1265 (2000).
31. Shulman, G. I. Cellular mechanisms of insulin resistance. *J. Clin. Invest.* **106,** 171–176 (2000).
32. Brownlee, M. Biochemistry and molecular cell biology of diabetic complications. *Nature* **414,** 813–820 (2001).
33. Lochhead, P. A. *et al.* 5-aminoimidazole-4-carboxamide riboside mimics the effects of insulin on the expression of the 2 key gluconeogenic genes PEPCK and glucose-6-phosphatase. *Diabetes* **49,** 896–903 (2000).
34. Hotamisligil, G. S., Shargill, N. S. & Spiegelman, B. M. Adipose expression of tumor necrosis factor-alpha: direct role in obesity-linked insulin resistance. *Science* **259,** 87–91 (1993).
35. Wellen, K. E. & Hotamisligil, G. S. Inflammation, stress, and diabetes. *J. Clin. Invest.* **115,** 1111–1119 (2005).
36. Weisberg, S. P. *et al.* Obesity is associated with macrophage accumulation in adipose tissue. *J. Clin. Invest.* **112,** 1796–1808 (2003).
37. Xu, H. *et al.* Chronic inflammation in fat plays a crucial role in the development of obesity-related insulin resistance. *J. Clin. Invest.* **112,** 1821–1830 (2003).
38. Lumeng, C. N., Bodzin, J. L. & Saltiel, A. R. Obesity induces a phenotypic switch in adipose tissue macrophage polarization. *J. Clin. Invest.* **117,** 175–184 (2007).
39. Zhang, H. M. *et al.* Geldanamycin derivative ameliorates high fat diet-induced renal failure in diabetes. *PLoS ONE* **7,** e32746 (2012).
40. Li, S., Shin, H. J., Ding, E. L. & van Dam, R. M. Adiponectin levels and risk of type 2 diabetes: a systematic review and meta-analysis. *J. Am. Med. Assoc.* **302,** 179–188 (2009).
41. Pischon, T. *et al.* Plasma adiponectin levels and risk of myocardial infarction in men. *J. Am. Med. Assoc.* **291,** 1730–1737 (2004).
42. Pajvani, U. B. *et al.* Complex distribution, not absolute amount of adiponectin, correlates with thiazolidinedione-mediated improvement in insulin sensitivity. *J. Biol. Chem.* **279,** 12152–12162 (2004).
43. Luo, Z., Saha, A. K., Xiang, X. & Ruderman, N. B. AMPK, the metabolic syndrome and cancer. *Trends Pharmacol. Sci.* **26,** 69–76 (2005).

Supplementary Information is available in the online version of the paper.

Acknowledgements We thank N. Kubota, K. Hara, I. Takamoto, Y. Hada, T. Kobori, H. Umematsu, S. Odawara, T. Aoyama, Y. Jing, S. Wei, K. Soeda and H. Waki for technical help and support; and K. Miyata, Y. Nishibaba, M. Yuasa and A. Hayashi for technical assistance and support. This work was supported by a Grant-in-aid for Scientific Research (S) (20229008, 25221307) (to T.K.), Grant-in-aid for Young Scientists (A) (23689048) (to M.I.), Targeted Proteins Research Program (to T.K.), the Global COE Research Program (to T.K.), Translational Systems Biology and Medicine Initiative (to T.K.) and Translational Research Network Program (to M.O.-I.) from the Ministry of Education, Culture, Sports, Science and Technology of Japan. Funding Program for Next Generation World-Leading Researchers (NEXT Program) (to T.Y.) from Cabinet Office, Government of Japan.

Author Contributions M.O.-I., M.I., T.Y., T.H., K.-i.-H., K.M., M.Y., H.T., T.K-S., M.S., H.O., K.T. and A.T. performed experiments. T.K., T.Y., M.O.-I. and M.I. conceived the study. T.K., A.T., T.Y. and S.Y. supervised the study. T.Y., T.K., M.O.-I. and M.I. wrote the paper. All authors interpreted data.

Author Information Reprints and permissions information is available at www.nature.com/reprints. The authors declare no competing financial interests. Readers are welcome to comment on the online version of the paper. Correspondence and requests for materials should be addressed to T.K. (kadowaki-3im@h.u-tokyo.ac.jp) or T.Y. (tyamau-tky@umin.net).

progenitors express *bnl>GFP*. As progenitors continue along the DT, DT larval cells activate *bnl>GFP* expression one segment at a time from anterior to posterior, matching progenitor movement.

This dynamic *bnl* expression along the migration path is required for progenitor outgrowth. Knockdown of *bnl* expression by RNA interference (RNAi) in larval tracheal cells blocked migration and resulted in diminished or absent PAT (Fig. 3, B and C; fig. S7, A to C; and movie S2). Mosaic expression of *bnl RNAi* in small patches along the path (*23*) also arrested migration, so long as the patch encompassed the full DT circumference (Fig. 3D; fig. S7, D and E; and movies S3 and S4). Thus, Bnl is required all along the migration path, and the signal does not cross even short gaps.

Ectopic *bnl* expression in GFP-labeled clones of larval tracheal cells induced by *dfr-FLP* (*23*) redirected progenitor migration. Depending on the location of the clones, ectopic *bnl* caused incorrect exit from the niche, premature entry onto the DT, or wrong turns on the DT (Fig. 4, B to D). Dual clones induced bifurcation with groups of progenitors moving toward each ectopic *bnl* source (Fig. 4E). Clones in Tr3 and posterior metameres caused progenitors in these regions to leave the niche, even though they do not normally do so (Fig. 4, G and H, and fig. S8, D and E). When there was a large clone, progenitors migrated throughout the clone (Fig. 4F), implying that progenitors do not require a gradient and will spread to cover an entire region of cells expressing *bnl* at equivalent levels. When *bnl*-expressing clones failed to induce migration, the clones appeared to be too far from the progenitors or there was competition from another clone close by (fig. S8, A and B). Ectopic *bnl* expression within the progenitor cluster arrested migration (fig. S8C).

The results show that the embryonic tracheal inducer Bnl FGF guides tracheal progenitors out of the niche and into the posterior during tracheal metamorphosis. The source of Bnl is the larval tracheal branches destined for destruction, which serve both as the source of the chemoattractant and as the substratum for progenitor migration. Several days earlier in embryos, these larval tracheal branches were themselves induced by Bnl provided by neighboring tissues. But after embryonic development, most tracheal cells, including those in the decaying larval branches, downregulate *btl* FGFR expression (fig. S2A) and thus do not respond to (or sequester) the Bnl signal they later express. One of the most notable aspects of this larval Bnl is its exquisitely specific pattern in decaying larval branches, which presages progenitor outgrowth. It is unclear how Bnl expression is controlled, though it does not appear to require signals from migrating progenitors because the *bnl* reporter expression front progressed normally when progenitor outgrowth was stalled by a tracheal break (fig. S6C). Perhaps expression of Bnl involves gradients in the tracheal system or spatial patterning cues established during embryonic development in conjunction with temporal signals mediated by molting hormones.

Because the signal guiding progenitor migration is provided by tracheae destined for destruction, progenitors become positioned along the larval branches they replace (Fig. 4I). Perhaps during tissue repair and homeostasis, recruitment of adult stem or progenitor cells from the niche is similarly guided by signals from decaying tissue, thereby ensuring that new tissue is directed to the appropriate sites.

References and Notes

1. N. Barker, S. Bartfeld, H. Clevers, *Cell Stem Cell* **7**, 656–670 (2010).
2. G. B. Adams, D. T. Scadden, *Nat. Immunol.* **7**, 333–337 (2006).
3. A. Alvarez-Buylla, D. A. Lim, *Neuron* **41**, 683–686 (2004).
4. C. Blanpain, E. Fuchs, *Nat. Rev. Mol. Cell Biol.* **10**, 207–217 (2009).
5. E. Sancho, E. Batlle, H. Clevers, *Curr. Opin. Cell Biol.* **15**, 763–770 (2003).
6. G. L. Ming, H. Song, *Neuron* **70**, 687–702 (2011).
7. E. Nacu, E. M. Tanaka, *Annu. Rev. Cell Dev. Biol.* **27**, 409–440 (2011).
8. K. D. Poss, *Nat. Rev. Genet.* **11**, 710–722 (2010).
9. T. Matsuno, *Jap. J. Appl. Entomol. Zool.* **34**, 165–167 (1990).
10. G. Manning, M. A. Krasnow, in *The Development of* Drosophila melanogaster, M. Bate, A. Martinez-Arias, Eds. (Cold Spring Harbor Laboratory Press, Woodbury, NY, 1993), vol. 1, pp. 609–685.
11. M. Weaver, M. A. Krasnow, *Science* **321**, 1496–1499 (2008).
12. A. Guha, L. Lin, T. B. Kornberg, *Proc. Natl. Acad. Sci. U.S.A.* **105**, 10832–10836 (2008).
13. C. Pitsouli, N. Perrimon, *Development* **137**, 3615–3624 (2010).
14. M. Sato, Y. Kitada, T. Tabata, *Dev. Biol.* **318**, 247–257 (2008).
15. C. Ribeiro, M. Neumann, M. Affolter, *Curr. Biol.* **14**, 2197–2207 (2004).
16. L. Liu, W. A. Johnson, M. J. Welsh, *Proc. Natl. Acad. Sci. U.S.A.* **100**, 2128–2133 (2003).
17. K. Guillemin *et al.*, *Development* **122**, 1353–1362 (1996).
18. C. Klämbt, L. Glazer, B. Z. Shilo, *Genes Dev.* **6**, 1668–1678 (1992).
19. M. Reichman-Fried, B. Z. Shilo, *Mech. Dev.* **52**, 265–273 (1995).
20. D. Sutherland, C. Samakovlis, M. A. Krasnow, *Cell* **87**, 1091–1101 (1996).
21. J. Jarecki, E. Johnson, M. A. Krasnow, *Cell* **99**, 211–220 (1999).
22. M. Sato, T. B. Kornberg, *Dev. Cell* **3**, 195–207 (2002).
23. Materials and methods are available as supporting material on *Science* Online.
24. S. Hayashi *et al.*, *Genesis* **34**, 58–61 (2002).

Acknowledgments: We thank M. Weaver, M. Metzstein, and other lab members for advice and reagents. This work was supported by a Genentech Graduate Fellowship and a Ruth L. Kirschstein NIH training grant (F.C.) and the Howard Hughes Medical Institute.

Supplementary Materials

www.sciencemag.org/content/343/6167/186/suppl/DC1
Materials and Methods
Figs. S1 to S10
References (*25–39*)
Movies S1 to S4

4 June 2013; accepted 12 November 2013
10.1126/science.1241442

Mutational Analysis Reveals the Origin and Therapy-Driven Evolution of Recurrent Glioma

Brett E. Johnson,[1]* Tali Mazor,[1]* Chibo Hong,[1] Michael Barnes,[2] Koki Aihara,[3,4] Cory Y. McLean,[1]† Shaun D. Fouse,[1] Shogo Yamamoto,[3] Hiroki Ueda,[3] Kenji Tatsuno,[3] Saurabh Asthana,[5,6] Llewellyn E. Jalbert,[7] Sarah J. Nelson,[7,8] Andrew W. Bollen,[2] W. Clay Gustafson,[9] Elise Charron,[10] William A. Weiss,[1,9,10] Ivan V. Smirnov,[1] Jun S. Song,[11,12] Adam B. Olshen,[6,11] Soonmee Cha,[1] Yongjun Zhao,[13] Richard A. Moore,[13] Andrew J. Mungall,[13] Steven J. M. Jones,[13] Martin Hirst,[13] Marco A. Marra,[13] Nobuhito Saito,[4] Hiroyuki Aburatani,[3] Akitake Mukasa,[4] Mitchel S. Berger,[1] Susan M. Chang,[1] Barry S. Taylor,[5,6,11]‡ Joseph F. Costello[1]‡

Tumor recurrence is a leading cause of cancer mortality. Therapies for recurrent disease may fail, at least in part, because the genomic alterations driving the growth of recurrences are distinct from those in the initial tumor. To explore this hypothesis, we sequenced the exomes of 23 initial low-grade gliomas and recurrent tumors resected from the same patients. In 43% of cases, at least half of the mutations in the initial tumor were undetected at recurrence, including driver mutations in *TP53*, *ATRX*, *SMARCA4*, and *BRAF*; this suggests that recurrent tumors are often seeded by cells derived from the initial tumor at a very early stage of their evolution. Notably, tumors from 6 of 10 patients treated with the chemotherapeutic drug temozolomide (TMZ) followed an alternative evolutionary path to high-grade glioma. At recurrence, these tumors were hypermutated and harbored driver mutations in the RB (retinoblastoma) and Akt-mTOR (mammalian target of rapamycin) pathways that bore the signature of TMZ-induced mutagenesis.

The genetic landscape of tumors is continually evolving, which can be an impediment to the clinical management of cancer patients with recurrent disease (*1*, *2*). In contrast to the clonal evolution of hematological malignancies (*3*, *4*) and solid tumor metastases (*5–7*), the local regrowth of solid tumors after surgery occurs under a unique set of evolutionary pressures, which are further affected by adjuvant therapies. Through the acquisition of new mutations, residual tumor cells can progress to a more aggressive state. Grade II astrocytic gliomas are

particularly troublesome from this perspective. Although surgery is the standard of care, these invasive brain tumors typically recur (*8*). Many remain grade II at recurrence, while others progress to a higher histological grade with a poor prognosis (*9*). The incidence and timing of malignant progression are variable and unpredictable (*8*).

We undertook genome sequence analysis of initial and recurrent human gliomas to address two questions: (i) What is the extent to which mutations in initial tumors differ from their subsequent recurrent tumors? (ii) How does chemotherapy with temozolomide (TMZ), a drug commonly used in the treatment of glioma, affect the mutational profile of recurrent tumors? We sequenced the exomes of 23 grade II gliomas at initial diagnosis and their recurrences resected from the same patients up to 11 years later (table S1). We selected initial tumors of predominantly astrocytic histology that capture the full spectrum of glioma progression (histological grade II to IV at recurrence) and adjuvant treatment history. Tumor and matched normal DNA were sequenced to an average 125-fold coverage, enabling the sensitive detection of mutations down to a 10% variant frequency, small insertions and deletions, and DNA copy number alterations (CNAs) (Fig. 1A and tables S2 and S3) (*10*).

We identified an average of 33 somatic coding mutations in each initial tumor, of which an average of 54% were also detected at recurrence (shared mutations) (Fig. 1A). The shared mutations included those in *IDH1*, *TP53*, and *ATRX* in most but not all cases (fig. S1) (*11*–*13*). All other somatic mutations were identified only in the initial tumor or only in the recurrent tumor from a given patient (private mutations) and thus presumably arose later in tumor evolution. For example, mutations in *SMARCA4* were private to the initial or recurrent tumor in six of seven patients and therefore may confer a selective advantage in the context of preexisting early driver events (*14*, *15*). Overall, the initial and recurrent gliomas displayed a broad spectrum of genetic relatedness (fig. S2 and table S4). At one end of this spectrum were four patients whose tumors showed a pattern of linear clonal evolution; we infer that the recurrent tumors in these patients were seeded by cells bearing ≥75% of the mutations detected in the initial tumors (as in patient 27, Fig. 1B). At the other end of the spectrum, tumors from three patients showed branched clonal evolution; we infer that the recurrent tumors in these patients were seeded by cells derived from the initial tumor at an early stage of its evolution, as the recurrent tumors shared ≤25% of mutations detected in the initial tumors. Patient 17 was an extreme example of branched clonal evolution, as the initial and recurrent tumors shared only the *IDH1* R132H ($Arg^{132} \rightarrow His$) mutation (Fig. 1C). This further implicates *IDH1* mutations as an initiating event in low-grade gliomagenesis (*12*). Indeed, *IDH1* mutation was the only shared mutation in every patient—an observation that supports the current interest in IDH1 as a therapeutic target (*16*). Paired tumors from the remaining 16 patients formed a continuum between linear and branched clonal evolution. Together, these data illustrate the extent to which genetically similar low-grade gliomas diverge after surgical resection, and suggest that recurrences may emerge from early stages in the evolution of the initial tumor.

Many solid tumors, including glioblastoma (GBM), display intratumoral heterogeneity (*17*, *18*). For example, geographically distinct parts of the tumor may have different mutations. Intratumoral heterogeneity could be a confounding factor in estimates of genetic divergence when only one relatively small fraction of a tumor is sampled. To explore the extent of intratumoral heterogeneity in our cases, we first analyzed the *BRAF* V600E ($Val^{600} \rightarrow Glu$) mutation that was subclonal in the initial tumor of patient 18 and undetectable in the recurrent tumor by either exome sequencing or droplet digital polymerase chain reaction (PCR) (Fig. 1D and fig. S3) (*10*). *BRAF* V600E was present in three of six additional samples from geographically distinct regions of the initial tumor, whereas seven additional samples of the recurrence all lacked this mutation. These results suggest that the *BRAF*-mutant clone did not expand, despite the proliferative advantage typically conferred by this mutation. Such a finding contrasts sharply with the selection and outgrowth of subclonal drivers during the evolution of chronic lymphocytic leukemias (*3*).

Beyond the actionable *BRAF* mutation, we sequenced the exomes of additional, geographically distinct samples from three cases to further determine the extent to which apparently private mutations might be misclassified because of intratumoral heterogeneity. In patient 17, for whom all mutations except *IDH1* were private, intratumoral heterogeneity was observed in the initial and recurrent tumor. From the mutational profiles, however, we inferred that three samples of the initial tumor and four samples of the recurrence all derived from a common tumor cell of origin that possessed only an *IDH1* R132H mutation (Fig. 2A and table S5). Moreover, the recurrent tumor contained driver mutations in *TP53* and *ATRX* distinct from those observed in the initial tumor. We found no evidence of these new *TP53* or *ATRX* mutations in the initial tumor at allele frequencies of ~0.1% (figs. S3 and S4), implying convergent phenotypic evolution (*5*) via a strong ongoing selection for loss of these genes. The initial and recurrent tumors likely did not arise independently, as they also shared three somatic noncoding mutations (fig. S5). Thus, the initial and recurrent tumors were only distantly related and, despite the local and relatively rapid recurrence (fig. S6), exonic mutations other than *IDH1* R132H were only transiently present during the course of this patient's disease. Finally, we sequenced the exomes of additional distinct samples of the initial and recurrent tumors from patients 26 and 27, broadening our assessment of the impact of intratumoral heterogeneity on the reported genetic divergence. We found that only a small minority of private mutations were actually shared events (7%; table S3) (*10*). Intratumoral heterogeneity therefore could not explain the majority of the genetic divergence between the initial and recurrent tumors in our cohort, including the driver mutations in initial tumors that were undetected in their recurrence.

To investigate whether sequential recurrences from a single patient could each be traced to the same evolutionary stage of the initial tumor, we sequenced the exomes of the second and third recurrent tumors from patient 04 and constructed a disease phylogeny by clonal ordering (Fig. 2B, fig. S7, and table S5) (*5*, *19*). The initial tumor and three sequential local recurrences were clonally related, as indicated by the shared phylogenetic branch containing early driver mutations in *IDH1* and *TP53*. We infer that the tumor cells seeding the second recurrence branched off from the initial tumor at a slightly earlier evolutionary stage than the cells seeding the first recurrence. In contrast, the third recurrent tumor was a direct outgrowth of the second recurrence. These results show that branched and linear patterns of clonal evolution occurred at differing times in the same patient and are therefore not intrinsic properties of the tumor.

Beyond maximal, safe, surgical resection, there is currently no standard of care for patients with low-grade glioma; options include surveillance, adjuvant radiation alone, TMZ alone, or radiation and TMZ. TMZ is an alkylating agent that induces apoptosis in glioma cells and is sometimes used to defer or delay the use of radiation. However, there is currently no information on whether treatment of grade II astrocytomas with TMZ confers longer overall survival (*8*). Because TMZ is also mutagenic (*20*), we sought to determine how adjuvant chemotherapy with TMZ affects the mutational profile of recurrent tumors by comparing the initial low-grade gliomas to their recurrence after treatment. Although the initial tumors and most of the recurrent tumors in our cohort had 0.2 to 4.5 mutations per megabase (Mb) (*21*, *22*), 6 of the 10 patients treated with

[1]Department of Neurological Surgery, University of California, San Francisco, CA 94158, USA. [2]Department of Pathology, University of California, San Francisco, CA 94158, USA. [3]Genome Science Laboratory, Research Center for Advanced Science and Technology, University of Tokyo, Meguro-ku, Tokyo 153-8904, Japan. [4]Department of Neurosurgery, University of Tokyo, Bunkyo-ku, Tokyo 113-8655, Japan. [5]Department of Medicine, University of California, San Francisco, CA 94158, USA. [6]Helen Diller Family Comprehensive Cancer Center, University of California, San Francisco, CA 94158, USA. [7]Department of Bioengineering and Therapeutic Sciences, University of California, San Francisco, CA 94158, USA. [8]Department of Radiology and Biomedical Imaging, University of California, San Francisco, CA 94158, USA. [9]Department of Pediatrics, University of California, San Francisco, CA 94158, USA. [10]Department of Neurology, University of California, San Francisco, CA 94158, USA. [11]Department of Epidemiology and Biostatistics, University of California, San Francisco, CA 94158, USA. [12]Institute for Human Genetics, University of California, San Francisco, CA 94158, USA. [13]Michael Smith Genome Sciences Centre, British Columbia Cancer Agency, Vancouver, BC V5Z 4E6, Canada.

*These authors contributed equally to this work.
†Present address: 23andMe Inc., Mountain View, CA 94043, USA.
‡Corresponding author. E-mail: jcostello@cc.ucsf.edu (J.F.C.); barry.taylor@ucsf.edu (B.S.T.)

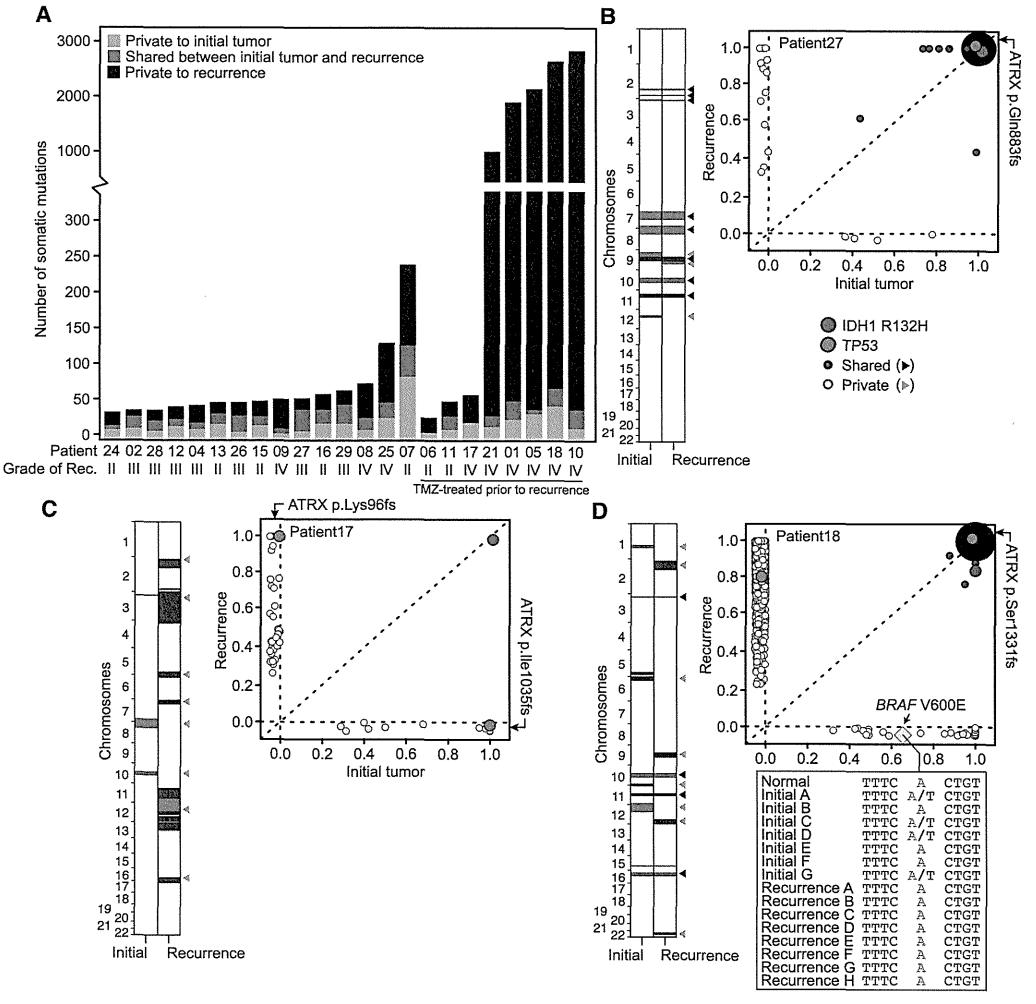

Fig. 1. Genetic landscapes of low-grade gliomas and their patient-matched recurrences. (**A**) Total number of mutations private to or shared between the initial and first recurrent glioma of 23 patients. (**B** to **D**) Shared and private somatic mutations in paired initial and recurrent tumors (*x* and *y* axes, respectively) as a function of the estimated fraction of tumor cells carrying the mutant allele. Mutations present in all the cells in both tumors are represented by a single point whose radius is scaled by the log count of such mutations. Shared and private CNAs are indicated (red and blue are gains and losses, respectively; white is copy-neutral). In (C), clonal *TP53* and *ATRX* mutations in the initial tumor were not identified in the recurrent tumor, but different clonal mutations in these two genes were acquired. (D) Inset shows the DNA sequence encompassing *BRAF* V600E in the normal tissue and in 15 geographically distinct samples of the initial and recurrent tumors.

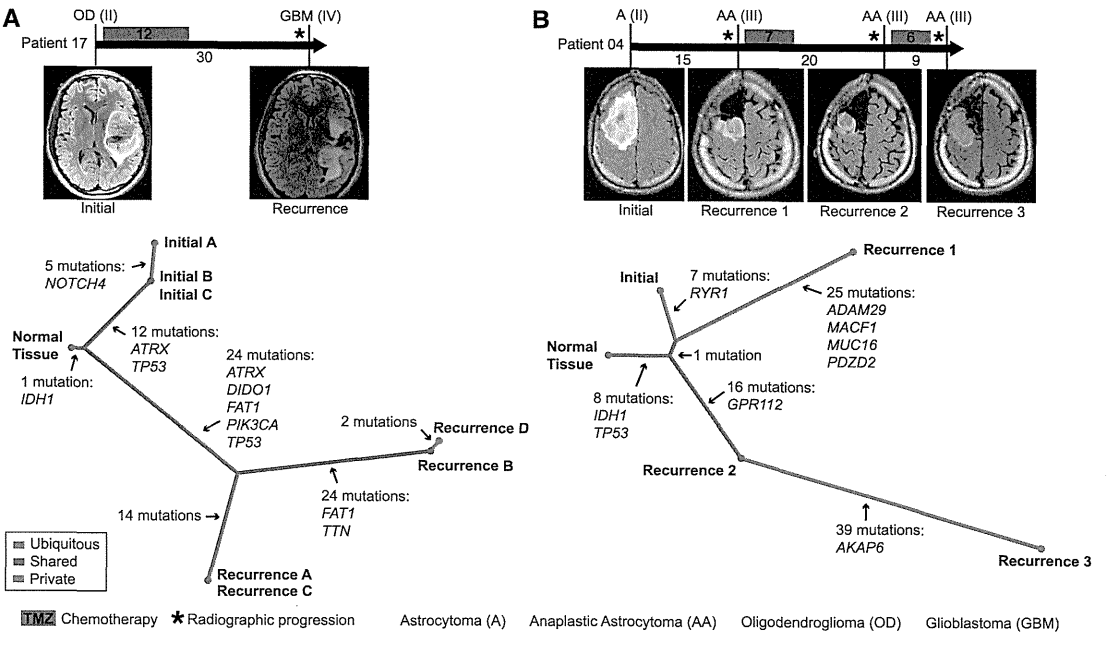

Fig. 2. Temporal and spatial patterns of clonal evolution in the tumors of two glioma patients. (**A** and **B**) A timeline of treatment histories for patient 17 (A) and patient 04 (B) (top, intervals labeled in months). Vertical bars correspond to the time of tumor resection and are labeled with the tumor diagnosis and grade. Representative MRIs are also shown. A phylogenetic tree (bottom) depicts the patterns of clonal evolution of these tumors inferred from the pattern and frequency of somatic mutations, highlighting genes frequently mutated in cancer.

TMZ had recurrent tumors that were hypermutated; that is, they harbored 31.9 to 90.9 mutations per Mb (table S6). Overall, 97% of these were C>T/G>A transitions predominantly occurring at CpC and CpT dinucleotides, which is a signature of TMZ-induced mutagenesis distinct from nonhypermutated tumors (fig. S8) (*20*, *22*, *23*). We classified C>T/G>A transitions in each hypermutated tumor as TMZ-associated if they were undetected in the matched initial tumor, which was resected before TMZ treatment (Fig. 3A). Although it is difficult to definitively attribute any single mutation to TMZ exposure, comparing the C>T/G>A mutation rates in each tumor pair suggested that >98.7% are due to TMZ-induced mutagenesis (*10*). To determine whether intratumoral heterogeneity in initial tumors resulted in the misclassification of some mutations as TMZ-associated, we sequenced the exomes of three additional geographically distinct samples of the untreated initial tumor from patient 18. For mutations classified as TMZ-associated, sequencing reads with the mutation were rare in the additional exomes and were found at rates no higher than expected by chance ($1.7 \pm 0.08\%$; $P = 0.5$, Wilcoxon rank-sum test) (*10*), further suggesting that they are induced by TMZ.

Resistance to TMZ develops in part through the acquisition of mutations that inactivate the DNA mismatch repair (MMR) pathway. MMR pathway dysfunction and continued TMZ exposure can in turn result in hypermutation (*22*–*25*). Indeed, we found that hypermutated tumors acquired somatic mutations in MMR genes that were not detected in their initial tumors, as well as aberrant DNA methylation of O^6-methylguanine-DNA methyltransferase (MGMT) (fig. S3, fig. S9, and table S1).

The introduction of thousands of de novo mutations may drive the evolution of TMZ-resistant glioma cells to higher states of malignant potential (*1*, *23*). Indeed, all six recurrent tumors that showed evidence of TMZ-induced hypermutation underwent malignant progression to GBM, a high-grade tumor with a worse prognosis (*8*, *9*). To investigate this hypothesis and to identify TMZ-associated mutations that may drive the outgrowth of GBM from low-grade glioma, we focused on the RB and Akt-mTOR signaling pathways, which are associated with high-grade gliomas (Fig. 3B) (*22*, *26*–*28*). In each hypermutated recurrence, TMZ-associated mutations affected genes coding for essential signaling molecules in these two pathways. For example, in the RB pathway we identified a TMZ-associated RB1 c.2520+1G>A splice-site mutation found previously in the germ line of patients with hereditary retinoblastoma (*29*, *30*). Transcriptome sequencing confirmed that this mutation triggered aberrant splicing, premature termination, and loss of the RB1 C-terminal domain necessary for growth suppression (Fig. 3C) (*31*). Recurrent tumors from patients 05 and 10 each had a TMZ-associated *CDKN2A* $Pro^{114} \rightarrow Leu$ mutation, which prevents $p16^{INK4A}$ protein encoded by this gene from inhibiting CDK4 or inducing cell cycle arrest (*32*). The same mutation has been reported in other tumor types (*33*) and in the germ line of patients with familial melanoma (*34*). Gene set enrichment analysis further confirmed the deregulation of RB1-mediated cell cycle control upon tumor recurrence (Fig. 3D), which suggests that TMZ-associated mutations compromise the function of the RB tumor suppressor pathway.

We also investigated TMZ-associated mutations that may activate the Akt-mTOR signaling pathway. We identified a TMZ-associated mutation (*PIK3CA* $Glu^{542} \rightarrow Lys$) in the recurrent tumor of patient 18 that drives Akt hyperactivation and induces mTOR-dependent oncogenic transformation (*35*). Similarly, the TMZ-treated second recurrence of patient 24 had TMZ-associated mutations in *PTEN* ($Ala^{121} \rightarrow Thr$ and $Gly^{165} \rightarrow Arg$) at residues critical to its phosphatase activity (*36*) that are recurrently mutated in GBM (*33*). Finally, we validated in vitro that a TMZ-associated *MTOR* S2215F ($Ser^{2215} \rightarrow Phe$) mutation in the recurrent tumor of patient 01 was constitutively

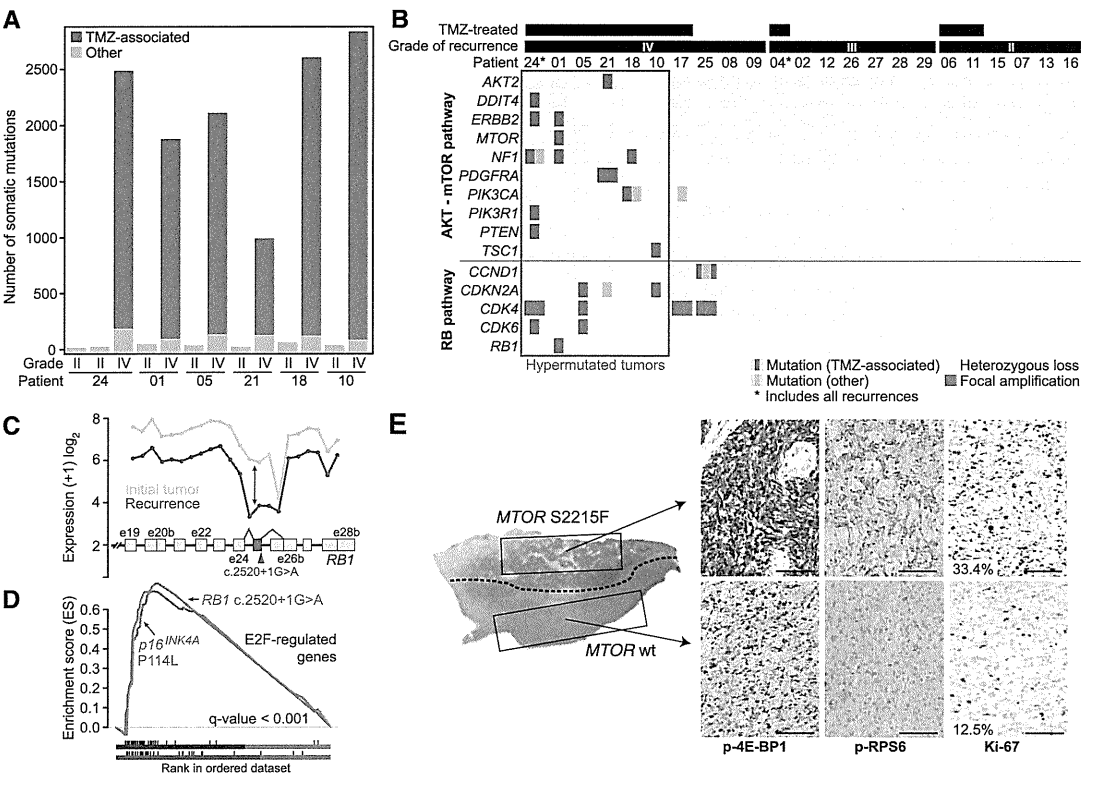

Fig. 3. Recurrent tumors from patients treated with TMZ harbor genetic alterations in the RB and Akt-mTOR signaling pathways. (**A**) Numbers of TMZ-associated mutations and other mutations identified in the six patients with hypermutated recurrent tumors. (**B**) Somatic mutations and CNAs acquired upon recurrence in key genes of pathways associated with GBM. (**C**) Expression level of *RB1* at each exon and exon-exon junction in the initial and recurrent tumor of patient 01 showing aberrant splicing of the *RB1* transcript in the recurrent tumor harboring the *RB1* c.2520+1G>A splice-site mutation. The *RB1* exon and exon junctions with significant differential usage (red) and the location of the splice-site mutation are shown. (**D**) Gene set enrichment analysis shows significant enrichment of genes down-regulated by *RB1* and up-regulated by *E2F* in the recurrent tumors of patients 01 (blue) and 10 (green), coincident with the acquisition of TMZ-associated mutations in the RB pathway. (**E**) Hematoxylin and eosin (H&E)–stained tumor sample from the first recurrent tumor of patient 01. A dotted line separates the two morphologically distinct regions. Immunohistochemistry (IHC) for phospho-RPS6, phospho-4E-BP1, and Ki-67 shows differential activation of mTORC1 targets and proliferation rates in the two adjacent regions. Scale bars, 100 μm.